Fronts in the wake of a parameter ramp: slow passage through pitchfork and fold bifurcations

Ryan Goh,* Tasso J. Kaper,† Arnd Scheel,‡ Theodore Vo§

December 16, 2022

Abstract

This work studies front formation in the Allen-Cahn equation with a parameter heterogeneity which slowly varies in space. In particular, we consider a heterogeneity which mediates the local stability of the zero state and subsequent pitchfork bifurcation to a non-trivial state. For slowly-varying ramps which are either rigidly propagating in time or stationary, we rigorously establish existence and stability of positive, monotone fronts and give leading order expansions for their interface location. For non-zero ramp speeds, and sufficiently small ramp slopes, the front location is determined by the local transition between convective and absolute instability of the base state and leads to an O(1) delay beyond the instantaneous pitchfork location before the system jumps to a nontrivial state. The slow ramp induces a further delay of the interface controlled by a slow-passage through a fold of strong- and weak-stable eigenspaces of the associated linearization. We introduce projective coordinates to de-singularize the dynamics near the trivial state and track relevant invariant manifolds all the way to the fold point. We then use geometric singular perturbation theory and blow-up techniques to locate the desired intersection of invariant manifolds. For stationary ramps, the front is governed by the slow passage through the instantaneous pitchfork bifurcation with inner expansion given by the unique Hastings-McLeod connecting solution of Painlevé's second equation. We once again use geometric singular perturbation theory and blow-up to track invariant manifolds into a neighborhood of the non-hyperbolic point where the ramp passes through zero and to locate intersections.

Keywords: Allen-Cahn, invasion front, slow parameter ramp, geometric singular perturbation theory, geometric blow-up, bifurcation delay

Mathematics Subject Classification: 34E15, 34E13 , 35B25, 35B36,

1   Introduction

The interaction of coherent structures, such as fronts, patterns, and waves, with spatio-temporal heterogeneity has recently attracted much interest in many scientific domains. Generally, one is interested how heterogeneities can nucleate, perturb, and mediate structures formed in a system. One such process which particularly motivates this work is that of directional quenching. Here, a heterogeneity travels across a medium, either controlled by the experimenter or another part of the system, rendering a stable equilibrium state unstable and hence nucleating the formation of a coherent structure in its wake. The speed and shape of the quenching mechanism then directly controls the structure formed in the wake. Examples of such mechanisms arise in fluid systems, phase-separative systems, chemical reactions, as well as biological applications; see [13] for a recent review.

While the quenching heterogeneity often varies sharply in space, so that that medium is rendered strongly unstable at the quenching location, heterogeneities which are slowly varying in space are also prevalent in many applications. To name a few specific examples, we mention wavenumber selection in Rayleigh-Benard convection with slowly varying Rayleigh constant [27, 37], oscillations in fluid flow past a slowly developing obstacle [22, 5],

---

*Department of Mathematics and Statistics, Boston University, 111 Cummington Mall, Boston, MA 02215, USA; `rgoh@bu.edu`.
†Department of Mathematics and Statistics, Boston University, 111 Cummington Mall, Boston, MA 02215, USA.
‡School of Mathematics, University of Minnesota, 206 Church St. SE, Minneapolis, MN 55455, USA.
§School of Mathematics, Monash University, Clayton, Victoria 3800, Australia

stripe orientation in morphogenesis due to gradients in production rates and parameters [20], and formation of cortex domain boundaries via spatially varying signal gradients [11]. See also [30] for theory about patterns in slowly varying environments and more applications. A different but related set of phenomena arise in slowly-varying temporal heterogeneities, where pattern-formation is dynamically mediated with the slow evolution of some parameter, with examples arising in ecological systems [38], soft-matter defects [41], and cosmological studies [25, 43]. Here the background medium is slowly rendered unstable in some fashion leading to a variety of effects, such as the selection of a specific wavenumber of striped pattern, the pinning of a front interface between two states at a certain location, or also the suppression of defect formation throughout the resulting coherent structure. See also [26] and references therein for a recent review of related problems of pattern formation on time-varying domains.

Allen-Cahn model equation In this work, we wish to rigorously study front solutions in a prototypical partial differential equation with a slowly-varying directional-quenching mechanism. We study such fronts in the scalar Allen-Cahn equation as it will serve as an approachable but still relevant setting to rigorously characterize the interaction of the front with the slowly varying quench, without dealing with unnecessary technical complications of more realistic equations. We expect our results to have bearing on similar interactions in other prototypical pattern forming systems with supercritical nonlinearities such as the Ginzburg-Landau equation and the Swift-Hohenberg equation, as well as more realistic models for the phenomena mentioned above. We also remark that the sharp quenched case has been considered in Allen-Cahn, in both one- and two-spatial dimensions, in the works [33, 32]. Our equation takes the form

$$u_t = u_{xx} + \mu(x - ct)u - u^3, \quad (x, t) \in \mathbb{R} \times \mathbb{R}_+, \tag{1.1}$$

$$\mu(\xi) := -\tanh(\epsilon\xi), \quad 0 < \epsilon \ll 1. \tag{1.2}$$

Here, as ϵ is small, the parameter heterogeneity, or "ramp", slowly varies from -1 at $\xi := x - ct = +\infty$ to 1 at $\xi = -\infty$, making the equilibrium $u = 0$ locally stable for $\xi := x - ct > 0$ and locally unstable for $\xi = x - ct < 0$. Further, c is an external control parameter which controls the speed at which the quench rigidly propagates through the medium. This particular quenching function is chosen as it is the solution of a simple first-order differential equation (1.4). While this quenching function simplifies the technical analysis, we expect similar phenomena to occur in a neighborhood of $\mu = 0$ with other slowly varying quenching terms, such as $\mu(\xi) = -\epsilon\xi$.

We study the formation of traveling front solutions $u(x - ct)$ which converge to 0 at $x \to +\infty$ and 1 at $x \to -\infty$. Front solutions of this type satisfy the autonomous travelling wave ordinary differential equation

$$0 = u_{\xi\xi} + cu_\xi + \mu u - u^3, \tag{1.3}$$

$$0 = \mu_\xi + \epsilon(1 - \mu^2), \quad \mu(0) = 0. \tag{1.4}$$

We report on front solutions for quenching speeds $c \in [0, 2)$, beginning with the dynamic quench with $c \in (0, 2)$ in Sections 1.1-1.2, and then for the stationary quench $c = 0$ in Sections 1.3-1.4.

1.1 Fronts formed by a dynamic quench with $c \in (0, 2)$: Phenomena and numerics

The moving fronts created by a dynamic quench with $c \in (0, 2)$ may be understood heuristically and numerically, as follows. Figure 1.1 depicts front solutions to (1.3)-(1.4) obtained through numerical continuation in AUTO07p [9] for a range of ϵ and c values. For $\mathcal{O}(1)$ values of $c \in (0, 2)$, we observe that, for large negative ξ, the solution tracks the quasi-stationary, or frozen coefficient, equilibrium value $\sqrt{\mu(\xi)}$. At some negative value of ξ, the solution profile quickly jumps down to values close to zero. We will later refer to this location as the front interface and denote the corresponding μ and ξ-values as μ_{fr} and ξ_{fr}, respectively; see (1.13). For $\mathcal{O}(1)$ values of $c > 0$ and for $0 < \epsilon \ll 1$, the central observation is that the front remains close to zero for an interval of length $\mathcal{O}(1)$ in μ, or $\mathcal{O}(\epsilon^{-1})$ in $\xi < 0$, where $\mu(\xi) > 0$ and the trivial state is unstable. The leading-order size of this interval may be determined asymptotically, by studying the transition from absolute to convective instability.

Absolute instability and the leading-order front interface The leading order spatial delay in growth in the front interface behind the quenching threshold $\mu = 0$ is controlled by the transition between convective and absolute instability of the trivial state as μ increases towards 1 for decreasing ξ. We note this behavior was also observed and non-rigorously studied in the work [5]. To understand this in heuristic terms, consider the PDE (1.1), posed in the co-moving frame $\xi = x - ct$, with initial condition close to the trivial state
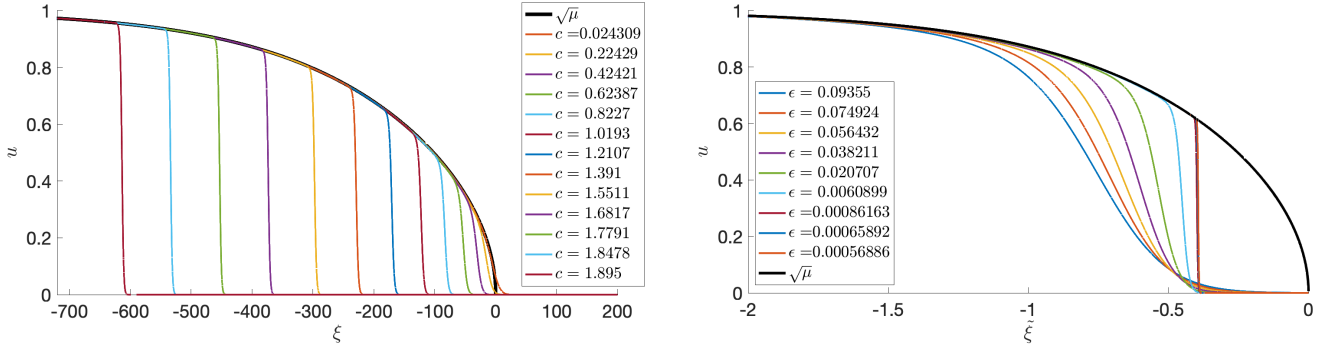
2

Figure 1.1: Results of numerical continuation of the traveling wave of (1.3)-(1.4) using AUTO07p. Left: Solutions $u(\xi)$ for a range of c-values (values in legend) with $\epsilon = 0.0025$ fixed. Right: Solutions u against the rescaled variable $\tilde{\xi} = \epsilon\xi$ for a range of ϵ values (values in legend) with $c = 1.2$ fixed, along with $\mu(\tilde{\xi})^{1/2}$ for $\tilde{\xi} < 0$.
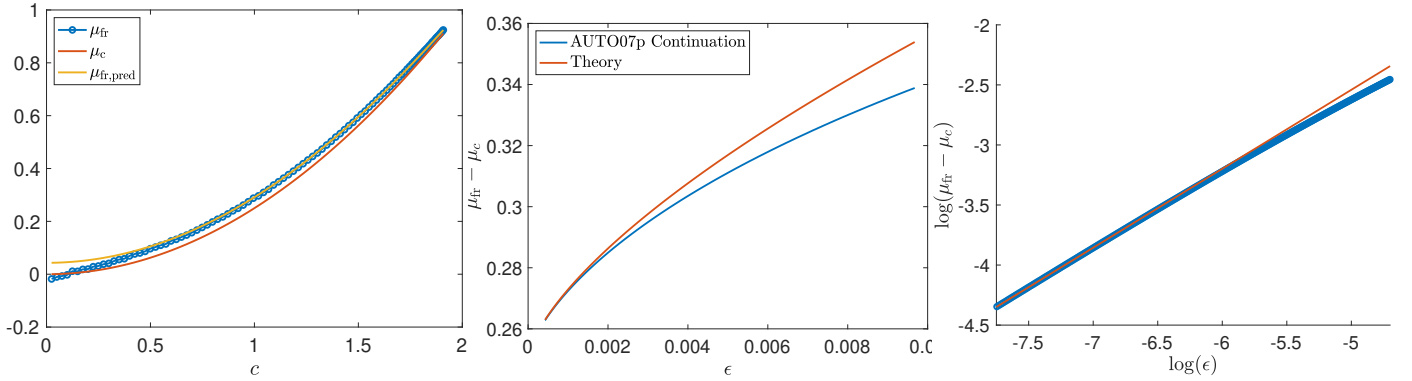

Figure 1.2: The front location μ_{fr} obtained from numerical simulations and compared to the theoretical prediction $\mu_{\mathrm{fr,pred}}$. Left: plot of μ_{fr} (blue circles), μ_c (orange line), and $\mu_{\mathrm{fr,pred}}$ (yellow line) given by the expansion (1.14) from Theorem 1 for a range of c values with $\epsilon = 0.0025$ fixed. Center: plot of $\mu_{\mathrm{fr}} - \mu_c$ comparing numerics (blue) and theoretical prediction (1.14) (orange) for $c = 1.2$. Right: Log-Log plot of $\mu_{\mathrm{fr}} - \mu_c$ against ϵ (blue), with linear fit (orange) of 10 left-most data points, also for $c = 1.2$. The measured slope is 0.650.

except for a small localized perturbation centered around some $\xi > 0$. As time increases, the perturbation will decay and be convected leftward until it reaches $\xi < 0$ when it will start to weakly grow while still being convected leftward. Thus, at each fixed small $\xi < 0$ the perturbation will decay pointwise. This behavior will continue for more negative ξ until μ is sufficiently large to induce pointwise growth, after which the front will grow to the non-trivial nonlinear state. This transition in growth type is known as the transition between convective and absolute instability.

To further understand this, we briefly digress to summarize the concepts of absolute and convective instability of an equilibrium state. For more detailed discussions see [39]. Consider the homogeneous Allen-Cahn equation, with μ a fixed constant, linearized around the trivial equilibrium $u = 0$, and posed in the co-moving frame with speed c,

$$v_t = v_{\xi\xi} + cv_\xi + \mu v =: L(\mu, c)v \tag{1.5}$$

The trivial state is *convectively unstable* if, for given $\mu, c > 0$, a localized perturbation grows but is convected into the bulk at $\xi = -\infty$, or in other words, the trivial state is unstable in the L^2-norm while locally at each point small perturbations decay over time. The state is *absolutely unstable* if localized perturbations grow both in the L^2-norm and pointwise. This transition can be located by studying the associated linear dispersion relation, obtained by inserting the ansatz $e^{\lambda t + \nu \xi}$ into (1.5),

$$0 = d(\lambda, \nu, c) := \nu^2 + c\nu + \mu - \lambda. \tag{1.6}$$

In the case of the Allen-Cahn equation, the transition between different types of instability is then obtained by finding (μ, c) values for which the branch point $(\lambda_{\mathrm{br}}, \nu_{\mathrm{br}})$ of (1.6) is marginally stable. That is, a (λ, ν)-pair which solves

$$0 = d(\lambda, \nu, c), \ 0 = d_\nu(\lambda, \nu, c),$$

3

and satisfies $\mathrm{Re}\,\lambda_{\mathrm{br}} = 0$. Calculation gives

$$\lambda_{\mathrm{br}} = -c^2/4 + \mu, \ \nu_{\mathrm{br}} = -c/2,$$

so that the boundary between instabilities is given by the curve

$$\mu_c := c^2/4.$$

Returning to the inhomogeneous system, and posing the time-dependent equation in the co-moving frame, one expects perturbations of the trivial state located near $\xi = 0$ to grow but be convected leftwards until reaching a ξ value where $\mu(\xi) \geq \mu_c$. Here, they will also grow pointwise until being saturated at the level $u = \sqrt{\mu}$ through the nonlinear term. Thus, we define ξ_c to be the value such that $\mu(\xi_c) = c^2/4$.

Further analyzing the numerical results depicted in Figure 1.1, we find the slow-variation of the parameter ramp induces a secondary delay of instability and in the growth of the front, so that the front location, which we denote as ξ_{fr}, is less than ξ_c and the corresponding μ-value, which we denote as μ_{fr}, is larger than μ_c. The numerics indicate the μ-delay of the front interface varies like

$$\mu_{\mathrm{fr}} - \mu_c \sim \epsilon^{2/3},$$

consistent with our theoretical results below. Since $\mu \approx -\epsilon\xi$ for μ near 0, one would then expect the spatial delay to go like

$$\xi_c - \xi_{\mathrm{fr}} \sim \epsilon^{-1/3},$$

leaving a large plateau region where the front lies close to the now absolutely unstable trivial state. We discuss the implications of this delay on the stability of this front in Section 8.1.

For $c > 2$, the trivial state is absolutely stable for all $\mu \leq 1$, hence small perturbations of the trivial state will be convected to negative infinity, and hence no front solution with this speed will exist. In the original PDE, we expect such perturbations to grow and spread through the domain with asymptotic speed 2. It is of interest how the slowly varying quench alters the convergence of the front speed to this asymptotic rate. We briefly discuss this in Section 8.4.

1.2 Main existence result for dynamic fronts $c \in (0, 2)$

As discussed above, we seek traveling wave solutions to the system of ODEs (1.3)-(1.4) for $\mathcal{O}(1)$ values of $c \in (0, 2)$. To simplify the setting, we reverse the spatial direction and consider solutions in $\zeta := -\xi$. We obtain the following traveling wave equation with asymptotic boundary conditions

$$0 = u_{\zeta\zeta} - cu_\zeta + \mu u - u^3, \tag{1.7}$$

$$\mu_\zeta = \epsilon(1 - \mu^2), \tag{1.8}$$

$$\lim_{\zeta \to -\infty} u(\zeta) = 0 \quad \text{and} \quad \lim_{\zeta \to +\infty} (u(\zeta) - 1) = 0. \tag{1.9}$$

Note that now μ increases from -1 to 1 as ζ increases. Further, we remark that all figures below depicting various aspects of the phase-portrait have direction of time governed by ζ. The desired solutions of this system are heteroclinic orbits between the equilibria $(u_0, v_0, \mu_-) = (0, 0, -1)$ and $(u_+, v_+, \mu_+) = (1, 0, 1)$ in the following first-order system:

$$u_\zeta = v \tag{1.10}$$

$$v_\zeta = cv - \mu u + u^3 \tag{1.11}$$

$$\mu_\zeta = \epsilon(1 - \mu^2). \tag{1.12}$$

These heteroclinic orbits will be found in the intersection of the unstable manifold, $W^{\mathrm{u}}(0, 0, -1)$, of the former equilibrium and the stable manifold, $W^{\mathrm{s}}(1, 0, 1)$, of the latter equilibrium. Since both of these are two-dimensional and lie in a three-dimensional ambient phase space, we expect a one-dimensional intersection and hence a locally isolated heteroclinic trajectory for each ϵ small. Our result establishes the existence of such fronts and locates where their interface, or take off from the origin, is located. As observed in Figure 1.1, the front has a fast jump from the trivial state up to local value of $\sqrt{\mu}$ when μ is near $\mu_c = c^2/4$. Hence, to account for the c- and ϵ-dependence of the front, we define the μ-location of the front interface as

$$\mu_{\mathrm{fr}} = \inf\{\mu \ : \ u > \sqrt{\mu_c}/2\}. \tag{1.13}$$

4

Since μ is one-to-one, we can then define ζ_{fr} so that $\mu(\zeta_{\text{fr}}) = \mu_{\text{fr}}$. Our main result is stated below. See Figure 1.3 for a schematic of the phase portrait, with insets in blue depicting local phase portraits for the singular system $\epsilon = 0$ near the origin.

Theorem 1. *There exists an $\epsilon_0 > 0$ sufficiently small such that, for $0 < \epsilon \leq \epsilon_0$ and for any $\mathcal{O}(1)$ value of $c \in (0,2)$, system (1.10)-(1.12) has a heteroclinic orbit Γ_ϵ which lies in the transverse intersection of $W^u(0,0,-1)$ and $W^s(1,0,1)$. Furthermore, Γ_ϵ is monotone increasing in u, and there exists a small $\tilde{\delta} > 0$ independent of ϵ such that Γ_ϵ is close to $(u,v) = (0,0)$ for $\mu \in [-1, \frac{c^2}{4} - \tilde{\delta})$ and Γ_ϵ is close to $(u,v) = (\sqrt{\mu},0)$ for $\mu \in (\frac{c^2}{4} + \tilde{\delta}, 1]$. The front location is given by*

$$\mu_{\text{fr}} = \frac{c^2}{4} + \Omega_0 \left(1 - \frac{c^4}{16}\right)^{\frac{2}{3}} \epsilon^{\frac{2}{3}} + \mathcal{O}(\epsilon \ln(\epsilon)). \tag{1.14}$$

Here, Ω_0 is the smallest positive zero of the following combination of Bessel functions of the first kind, $J_{-1/3}(2z^{3/2}/3) + J_{1/3}(2z^{3/2}/3)$.

This theorem establishes the main result about quenched fronts for all $\mathcal{O}(1)$ values of $c \in (0,2)$, showing that the monotone invasion fronts have interfaces located at $\mu = c^2/4$ to leading order, and not at $\mu = 0$, *i.e.*, not where the instantaneous pitchfork bifurcation occurs in which $u = 0$ becomes an unstable solution of the PDE. We observe that $\mu = c^2/4$ is where the unstable node, which is created at $\mu = 0$ in the instantaneous pitchfork bifurcation, becomes an unstable improper node, on its way to transitioning to being an unstable spiral. Hence, there is a substantial delay in the loss of stability of the $u = 0$ in the PDE. The leading-order term gives an $\mathcal{O}(1)$ delay in μ which corresponds to an $\mathcal{O}(\epsilon^{-1})$ delay in ζ. The next order term gives a further delay, where $\mu > \mu_c$ and the system is absolutely unstable, which is $\mathcal{O}(\epsilon^{2/3})$ in μ and thus $\mathcal{O}(\epsilon^{-1/3})$ in ζ. Moreover, in the proof of the theorem, we use a projectivized coordinate to track smoothly through $\mu = 0$ and all the way up through $\mu = c^2/4$. It turns out that there is a further delay in the loss of stability (*i.e.*, in μ_{fr}) beyond $c^2/4$, which is of $\mathcal{O}(\epsilon^{2/3})$ duration, and this arises due to a slow-passage through a fold bifurcation in the projectivized system.
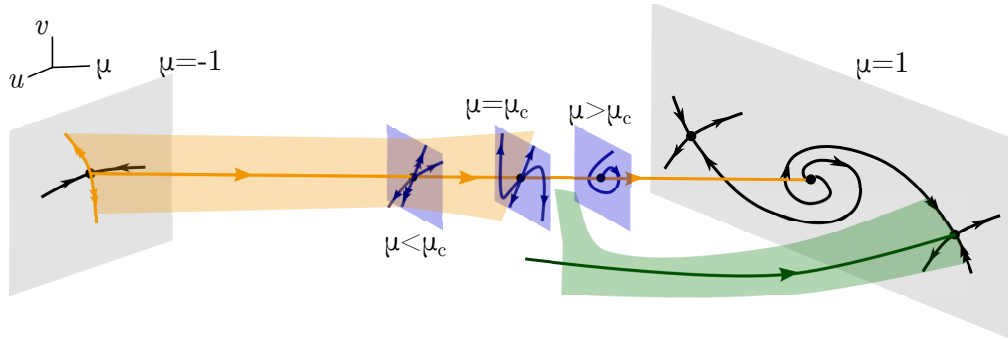

Figure 1.3: Schematic phase portrait for system (1.10)-(1.12) for $0 < \epsilon \ll 1$. Invariant planes $\{\mu = \pm 1\}$ depicted in grey, unstable manifold $W^u(0,0,-1)$ in orange, stable manifold $W^s(1,0,1)$ in green. Overlayed are $\mu = $ constant planes depicted in blue which are invariant for $\epsilon = 0$.

We use geometric singular perturbation theory to construct these heteroclinic orbits for each $\mathcal{O}(1)$ value of $c \in (0,2)$ in the singular limit $0 < \epsilon \ll 1$, first constructing the relevant manifolds for $\epsilon = 0$, where each plane $\{\mu = \text{constant}\}$ is invariant under the flow of (1.10)-(1.12). We use a projective blow-up near the line $\{(0,0,\mu)\,;\,\mu \in [-1,1]\}$ to track the manifolds $W^u(0,0,-1)$ and $W^s(1,0,1)$ to a neighborhood of the point $(0,0,\mu_c)$ where an intersection can be constructed. We use the projective coordinate $z = v/u$, in combination with u to track the evolution of linear subspaces near the origin as μ slowly varies. The eigenspaces of the $\epsilon = 0$ linear system are equilibria in the projective dynamics and collide in a fold bifurcation at μ_c. For larger μ, the corresponding eigenspaces become complex and hence the projective dynamics become oscillatory. This winding allows for subspaces to traverse more of the phase space, increasing the likelihood of an intersection. For $0 < \epsilon \ll 1$ these curves of equilibria perturb to normally hyperbolic invariant slow manifolds, with one-dimensional strong unstable fibers outside a neighborhood of μ_c. To get around the loss of normal hyperbolicity near μ_c, we use blow-up techniques to track the attracting slow-manifold and its unstable fibers around the fold where it can intersect $W^s(1,0,1)$.

1.3 Fronts created by a stationary quench ($c = 0$): Phenomena and numerics

A stationary quench is modeled by the PDE (1.1) with $c = 0$. Physically, the state $u = 0$ is linearly unstable on the negative half of the domain and stable on the positive half. For small non-negative initial data, a stationary front forms, and its profile is governed by the following spatial ODE:

$$u_{\xi\xi} = -\mu u + u^3, \qquad \mu_\xi = -\epsilon(1 - \mu^2), \qquad \mu(0) = 0, \tag{1.15}$$

where $\xi = x - ct$ reduces to $\xi = x$. The front interface is controlled by the slow spatial ramping through the pitchfork bifurcation, which occurs at $\xi = 0$, where $\mu = 0$. Indeed, in the three-dimensional $(u, v = u_\xi, \mu)$ phase space, system (1.15) with $\epsilon = 0$ has a pair of saddles at $(\pm\sqrt{\mu}, 0, \mu)$ and a center at $(0, 0, \mu)$ for each $\mu > 0$, and these merge in a pitchfork bifurcation at $\mu = 0$, so that there is only a saddle fixed point at the origin for each $\mu < 0$. Then, for $\epsilon > 0$ and small, solution profiles of (1.15) are depicted in Figure 1.4. The solutions lie near the curve $u = \sqrt{\mu}$ for large negative ξ, and near $u = 0$ for large positive ξ. In between, in a neighborhood of $\xi = 0$, the solutions slowly drop below $\sqrt{\mu}$ but then quickly rise above it, with the exponentially decaying tail of the front being located slightly ahead of the instantaneous bifurcation point $\mu = 0$. Hence, the front interface appears to lie ahead of $\mu = 0$. From a PDE perspective, this advance of the front is caused by the lack of a drift term so that diffusion connects the front through a decaying tail across $\xi = 0$.
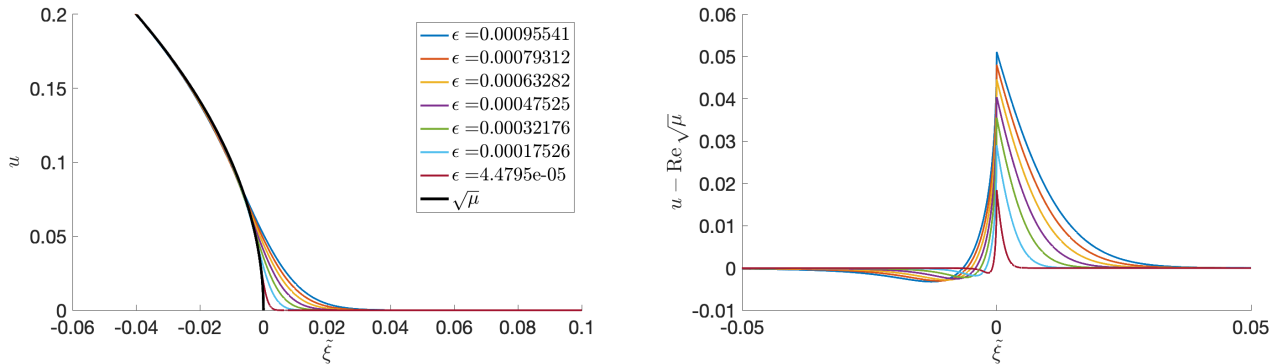

Figure 1.4: Left: the solutions of (1.15), i.e., the system with $c = 0$, for a range of small ϵ values, compared with $\sqrt{\mu}$ and zoomed in near $\xi = 0$; Right: the curves $u - \mathrm{Re}\sqrt{\mu}$ for the same range of ϵ values as in the left plot. Here $\tilde{\xi} = \epsilon\xi$.

It turns out that the second Painlevé equation [1, 6, 8] lies at the heart of system (1.15). This may be seen informally by deriving the leading order asymptotics for $0 < \epsilon \ll 1$ as follows. Substitute the closed form expression $\mu(\xi) = -\tanh(\epsilon\xi)$ into (1.15) to find $u_{\xi\xi} = \tanh(\epsilon\xi)u + u^3$. Next, scale $\eta = \epsilon^{1/3}\xi$ and $u = \sqrt{2}\epsilon^{1/3}\tilde{u}$, which corresponds to the significant degeneration of the equation in the neighborhood of $\xi = 0$ and $u = 0$ where the instantaneous pitchfork bifurcation occurs. The equation becomes $\tilde{u}_{\eta\eta} = \epsilon^{-2/3}\tanh(\epsilon^{2/3}\eta)\tilde{u} + 2\tilde{u}^3$, where the factor of $\sqrt{2}$ in the scaling of u has put the coefficient on the cubic term into standard form. Finally, Taylor expanding, one obtains

$$\tilde{u}_{\eta\eta} = (\eta + \mathcal{O}(\epsilon^{4/3}\eta^3))\tilde{u} + 2\tilde{u}^3. \tag{1.16}$$

Therefore, we see that, for any finite interval of values of η, the parameter ϵ can be taken to be small enough so that the equation is a perturbation of the second Painlevé equation (P_{II}),

$$w_{\eta\eta} = \eta w + 2w^3. \tag{1.17}$$

The key solution of interest here is the Hastings-McLeod solution, $w_{HM}(\eta)$ [18], which is the unique positive, monotone solution of (1.17) which decays as $\eta \to +\infty$ and satisfies $w_{HM}(\eta) \sim \sqrt{-\eta/2}$ as $\eta \to -\infty$. In more detail, it has the following asymptotics

$$w_{HM}(\eta) \sim \mathrm{Ai}(\eta) \quad \text{as } \eta \to \infty, \tag{1.18}$$

$$w_{HM}(\eta) \sim \sqrt{-\eta/2} \quad \text{as } \eta \to -\infty, \tag{1.19}$$

$$\frac{dw_{HM}}{dx}(\eta) < 0 \quad \text{for all } \eta. \tag{1.20}$$

Here, $\mathrm{Ai}(\eta)$ denotes the Airy function. We note that all solutions of (1.17) which decay to zero as $\eta \to +\infty$ satisfy $w(\eta) \sim k\mathrm{Ai}(\eta)$ as $\eta \to +\infty$ for some $k \in \mathbb{R}$. Parameterizing this family, $w_k(\eta)$, by $k \in \mathbb{R}$, we note that

$w_{\mathrm{HM}} = w_1(\eta)$ partitions this family into two distinct classes. For $|k| > 1$, the solution $w_k(\eta)$ decays in oscillatory fashion as $\eta \to -\infty$. For $|k| < 1$, the solution $w_k(\eta)$ has a pole at some finite point $\eta = c_0(k) < 0$. That is $w_k(\eta) \sim \mathrm{sign}(k)/(\eta - c_0(k))$ as $\eta \to c_0(k)^+$, where we note that $c_0(k) \to -\infty$ as $|k| \to 1^+$. Proofs of these results can be found in [18]; see also Chapter 32 of the Digital Library of Mathematical Functions [8, §32.11(ii)], as well as [3, 4]. Also note, by symmetry, the solution with $k = -1$ is the other separatrix, with asymptotics $w_{-1}(\eta) \sim -\sqrt{-\eta/2}$ as $\eta \to -\infty$.

We note the solution w_{HM} perturbs to a solution $\tilde{u}_{\mathrm{HM}}(\eta)$ of (1.16), which is the unique one satisfying the same asymptotic boundary conditions (1.18) - (1.20). Translating back to the original variables, we define

$$u_{HM}(\xi) = \sqrt{2}\epsilon^{1/3}w_{HM}(\epsilon^{1/3}\xi), \tag{1.21}$$

which, for each ϵ sufficiently small, formally gives the front of (1.15) to leading order on any finite interval about $\xi = 0$. The numerically obtained solutions of the full system are compared to this rescaled Hastings-McLeod solution in Figure 1.5.
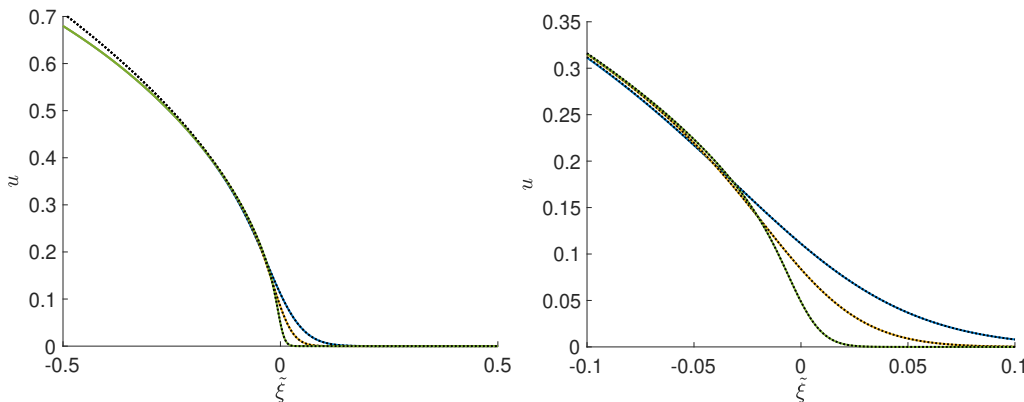

Figure 1.5: Left: front solutions as functions of $\tilde{\xi} = \epsilon\xi$ from numerical continuation for $\epsilon = 9.81*10^{-3}$ (blue solid), $\epsilon = 4.21*10^{-3}$ (yellow solid), and $\epsilon = 8.27*10^{-4}$ (green solid) with the rescaled connecting solution u_{HM} of (1.17) (black dashed). The blue, yellow, and green curves lie on top of each other for much of this plot. Right: zoom in of same solution profiles showing good agreement with the prediction u_{HM}. The numerical solution of (1.17) was obtained using the Matlab Chebfun package [10].

1.4 Existence result for stationary fronts with $c = 0$

With the above intuition in mind, we state the main result for $c = 0$. The equation (1.15) may be written as a third-order autonomous system,

$$u_\xi = v, \tag{1.22}$$
$$v_\xi = -\mu u + u^3, \tag{1.23}$$
$$\mu_\xi = -\epsilon(1 - \mu^2), \qquad \mu(0) = 0. \tag{1.24}$$

The front of (1.22)-(1.24) is a heteroclinic orbit connecting the fixed points $(u_+, v_+, \mu_+) = (1, 0, 1)$ to $(u_0, v_0, \mu_-) = (0, 0, -1)$, and it lies in the transverse intersection of the unstable and stable manifolds of these fixed points, respectively.

Theorem 2. *For each $\epsilon > 0$ sufficiently small, system (1.22)-(1.24) has a heteroclinic orbit (u^*, v^*, μ^*) in the transverse intersection of $W^u(1, 0, 1)$ and $W^s(0, 0, -1)$. Furthermore, there exists a small $\rho > 0$, independent of ϵ, such that the front satisfies*

$$u^*(\xi) = u_{HM}(\xi) + \mathcal{O}(\epsilon^{2/3}), \quad \text{for all } |\xi| \le \rho\epsilon^{-1/3}. \tag{1.25}$$

where $u_{HM}(\xi) = \sqrt{2}\epsilon^{1/3}w_{HM}(\epsilon^{1/3}\xi)$ and w_{HM} is the unique Hastings-McLeod solution of (1.17).

The estimate (1.25) implies that the scaled Hastings-McLeod solution gives the leading order inner solution in the region $|\mu| \le \rho\epsilon^{2/3}$. A comparison of the leading-order inner solution with the numerically-obtained front solutions for two small ϵ values is given in Figure 1.5. We add that, to make it easier to compare solutions for different ϵ, the solutions are plotted against the variable $\tilde{\xi} = \epsilon\xi$, and the leading order asymptotics take the form

$$u^*(\tilde{\xi}/\epsilon) \sim \epsilon^{1/3}w_{HM}(\epsilon^{-2/3}\tilde{\xi}), \qquad |\tilde{\xi}| \lesssim \epsilon^{2/3}. \tag{1.26}$$

This theorem is proven using geometric desingularization, or "blow-up" of system (1.22)-(1.24), near the point $(u, v, \mu) = 0$, where the critical manifolds for $\epsilon = 0$ lose hyperbolicity. Here this point is blown-up into a 3-sphere whose singular dynamics are controlled by Painlevé's second equation at leading order. We use inclination lemmas to track the desired invariant manifolds into a neighborhood of the sphere. We then use exponential trichotomies to lift the transversality of the Hastings-McLeod solution on the singular sphere and track $W^u(1, 0, 1)$ and $W^s(0, 0, -1)$ across the sphere and show they also intersect transversely.

As part of the analysis here of the fronts created by a stationary quench, we show that the Hastings-McLeod solution lies in the transverse intersection of invariant stable and unstable manifolds of (1.17). In the extended phase of (1.17), these manifolds consist of solutions which satisfy exponential growth and decay conditions as $\eta \to \infty$ and $w \to 0$ and of solutions satisfying exponential growth and decay conditions as $\eta \to -\infty$ and $w \to \sqrt{-\eta/2}$. As discussed above, the Hastings-McLeod solution is the unique solution of the Painlevé II equation which separates two different types of solutions. Namely, among all solutions that decay asymptotically proportionally to an Airy function as $z \to +\infty$, it separates those which undergo oscillatory decay as $z \to -\infty$ from those which have a simple pole at some negative value of z. These two different classes of solutions lie on different sides of the transverse intersection of the stable and unstable manifolds. Moreover, establishing this transverse intersection for (1.17) is also a natural building step for showing that the stationary front of the PDE (1.1) lies in the transverse intersection of invariant manifolds.

Physically, the Allen-Cahn type PDE studied here may also be viewed as a prototype system for studying more general problems in which there is a slowly-varying parameter ramp in space. Such situations arise for example in Taylor vortex flow when there is a time-independent parameter ramp which varies slowly in space [36, 35]. The governing equations are much more complex there, but experimental results and asymptotic analysis shows that the slowly-varying spatial ramp can induce the selection of a unique pattern [36, 37].

Remark 1.1. *The $c = 0$ case is an important example of slow passage through a super-critical pitchfork bifurcation in multiple time scale dynamical systems, with two fast variables and one slow variable. Indeed, this is a natural next step in the use of geometric desingularization to analyze dynamic pitchfork bifurcations, which has previously only been done for systems with one fast variable and one slow variable, see [29]. The geometry induced by the two fast variables requires the tracking of additional hyperbolic directions.*

Remark 1.2. *Earlier analyses of slow passage through pitchfork bifurcations have involved the case of a generic center equilibrium undergoing a slow dynamic pitchfork bifurcation in which the center becomes a saddle and two new centers emerge. In Hamiltonian mechanics, this corresponds to a single well potential slowly changing into a double well. These earlier analyses [16, 31] were carried out using singular perturbation theory and matched asymptotic expansions. In contrast, because the pitchfork bifurcation encountered here is of the opposite type, with a saddle point becoming a center and giving birth to two saddles (and as a result the full Allen-Cahn PDE transitions from one stable state to another), a rigorous analysis is possible by exploiting the hyperbolicity on both sides of $\mu = 0$ and by using geometric desingularization to study the loss of hyperbolicity in a neighborhood of $\mu = 0$. Also, in principle, one could use a complex time variable, obtain the formal asymptotic results here from the the earlier works [16, 31].*

1.5 Outline

The analysis of PDE (1.1) in the case of $c \in (0, 2)$ and the proof of Theorem 1 are presented in Sections 2-4. In particular, in Section 2, we set up our theoretical approach, define the projective coordinates, and describe the singular system with $\epsilon = 0$. In Section 3, we use Fenichel theory and geometric blow-up to unfold the dynamics and track the relevant invariant manifolds for $0 < \epsilon \ll 1$. Then, in Section 4, the desired heteroclinic intersection is established in a neighborhood of the dynamic fold, hence completing the proof of Theorem 1. Next, the analysis of PDE (1.1) in the case of $c = 0$ and the proof of Theorem 2 are presented in Sections 5-7. In Section 5, we begin the study of stationary fronts in the $c = 0$ case, using a geometric blow-up of a neighborhood of the instantaneous pitchfork bifurcation point. Then, Section 6 establishes that the Hastings-McLeod solution of (1.17) exists in the transverse intersection of invariant manifolds, and then that the singular heteroclinic representing the stationary front created by the quench also exists in the transverse intersection of invariant manifolds of the full system. The proof of Theorem 2 is completed in Section 7, by establishing the inclination properties of invariant manifolds, and showing that the transverse intersection exists for all $0 < \epsilon \ll 1$. In Section 8, we complement the proofs of Theorems 1 and 2 by giving an argument showing the fronts of Theorem 1 are nonlinearly asymptotically stable, discussing the existence of other, non-monotonic front solutions possible

in the wake of the quench for $c \in (0,2)$, and discussing parameter regimes not covered by our result, such as the $c, \epsilon \sim 0$ regime. We provide additional numerical results to motivate future studies, as well as discuss other slowly-varying heterogeneities which we expect to induce novel front invasion behavior.

2 Setup for traveling-waves with $c \in (0,2)$

In this section, and in Sections 3-4, we consider $\mathcal{O}(1)$ values of the speed $c \in (0,2)$. We linearize system (1.10) - (1.12) about the equilibria (u_0, v_0, μ_-) and (u_+, v_+, μ_+). The Jacobian at (u_0, v_0, μ_-) has eigenvalues

$$ \nu_{-,\epsilon} = 2\epsilon, \qquad \nu_{-,\pm} = \frac{c}{2} \pm \sqrt{\frac{c^2}{4} - \mu_-} = \frac{c}{2} \pm \sqrt{\frac{c^2}{4} + 1}. $$

Thus, it is a hyperbolic saddle with two-dimensional unstable manifold $W^{\mathrm{u}}(0,0,-1)$, whose tangent space is spanned by the vector $(1, \nu_{-,+}, 0)$ in the $\mu \equiv -1$ plane and by the vector $(0,0,1)^T$ in the direction of the μ−axis. Then, the Jacobian at (u_+, v_+, μ_+) has eigenvalues

$$ \nu_{+,\epsilon} = -2\epsilon, \quad \nu_{+,\pm} = \frac{c}{2} \pm \sqrt{\frac{c^2}{4} - \mu_+ + 3u_+^2} = \frac{c}{2} \pm \sqrt{\frac{c^2}{4} + 2}. $$

Thus, it is a hyperbolic saddle, with two-dimensional stable manifold, $W^{\mathrm{s}}(1,0,1)$, whose tangent space is spanned by the vector $(1, \nu_{+,-}, 0)^T$ in the $\mu \equiv 1$ plane and by the vector $(0,0,1)^T$ in the direction of the μ−axis. As mentioned above, we wish to locate intersections $W^{\mathrm{u}}(0,0,-1) \cap W^{\mathrm{s}}(1,0,1)$, which consists of a pair of two-dimensional manifolds in three dimensional space, indicating we generically expect a one-dimensional intersection of these manifolds and hence a locally unique trajectory for each $0 < \epsilon \ll 1$.

2.1 Projective coordinates/blow-up

For $\epsilon = 0$, each $\mu = $ constant plane is invariant with equilibria $(0,0,\mu)$ for all μ and $(\pm\sqrt{\mu}, 0, \mu)$ for $\mu \in [0,1]$. The latter are saddles for all $\mu \in (0,1]$. The former is a hyperbolic saddle for $\mu < 0$, degenerate unstable node for $\mu = 0$, unstable node for $\mu \in (0, c^2/4)$. It is a degenerate source for $\mu = c^2/4$ with two-dimensional Jordan block, and is an unstable spiral for $\mu \in (c^2/4, 1]$. We remark that the algebraically-double eigenvalue found at $\mu = c^2/4$ is also located using the double-root calculation given in Section 1.1 above. In order to unfold the dynamics near $(u,v) = (0,0)$ for $\mu \in [-1,1]$ and $0 < \epsilon \ll 1$, we perform a directional blowup in the variables

$$ \tilde{z} = v/u, \quad u. \tag{2.1} $$

See [21] for a recent work using a similar approach in a different context. These coordinates allow one to track the manifold $W^{\mathrm{u}}(0,0,-1)$ from $\mu = -1$ through the change in linear stability at $\mu = 0$ and through the Jordan block at $\mu = c^2/4$.

In the coordinates (2.1), the system (1.10)–(1.12) becomes

$$ \tilde{z}_\zeta = -\tilde{z}^2 + c\tilde{z} - (\theta + c^2/4) + u^2, \tag{2.2} $$

$$ u_\zeta = \tilde{z}u, \tag{2.3} $$

$$ \theta_\zeta = \epsilon(1 - (\theta + c^2/4)^2), \tag{2.4} $$

where we have also set $\theta := \mu - c^2/4$ to translate the point $\mu = c^2/4$ to the origin. Here, $\mu_+ = 1$ corresponds to $\theta_+ := 1 - c^2/4$ and $\mu_- = -1$ to $\theta_- := -1 - c^2/4$.

Remark 2.1. *In order to unfold the dynamics in the region near the origin, one generally would blow up the line of equilibria $(0,0,\mu)$ into a cylinder via a polar coordinate blow up $u = r\cos\phi$, $v = r\sin\phi$. Such a coordinate change, while elucidating the small amplitude dynamics, would push the non-trivial equilibria $(u,v) = (\sqrt{\mu},0)$ away to infinity in the limit $r \to 0$, requiring multiple coordinate charts to construct the intersection. Hence, we instead perform a directional blow-up, projecting the dynamics on different charts of the cylinder using blow-up in both the u and v directions, $\tilde{z} = v/u$, u and $\tilde{w} = u/v$, v, respectively. We find that only the first chart is required to construct the monotonic front given in Theorem 1. We also note that both charts, or the aforementioned cylindrical blow-up, would be needed to construct non-monotonic fronts with oscillatory tails. See Section 8.2 and Figure 8.1 for more discussion on the non-monotonic fronts.*

There are several key features of system (2.2)-(2.4). A central feature is that the plane

$$U_0 = \{u = 0\} \tag{2.5}$$

is invariant for all $\epsilon \geq 0$. With $\epsilon = 0$, θ is a constant, and U_0 contains the equilibria of (2.2)-(2.4), which are at $(\tilde{z}, u, \theta) = (\tilde{z}_\pm(\theta), 0, \theta)$ for each $\theta \in [-1 - c^2/4, 0]$. Here, $\tilde{z}_\pm$ satisfies

$$-\tilde{z}^2 + c\tilde{z} - (\theta + c^2/4) = 0, \quad \mathrm{Re}\, \tilde{z}_+ \geq c/2.$$

These equilibria collide in a saddle-node bifurcation at $\theta = 0$ (that is $\mu = c^2/4$) and $\tilde{z} = c/2$. Also, at $\theta = -c^2/4$ (that is $\mu = 0$) there is a pitchfork bifurcation from the point $(\tilde{z}_-, 0, \theta)$ in which a branch of equilibria emerges

$$(\tilde{z}_*, u_*, \theta) = (0, \sqrt{\theta + c^2/4}, \theta), \qquad \theta \in (-c^2/4, 1 - c^2/4].$$

These lie out of the plane U_0 and correspond to the non-trivial state $(u, v) = (\sqrt{\mu}, 0)$. Due to reversibility, there is also a branch of equilibria $(0, -\sqrt{\theta + c^2/4}, \theta)$ for the same interval of fixed θ values, which correspond to the other non-trivial state $(u, v) = (-\sqrt{\mu}, 0)$ that also bifurcates at $\theta = -c^2/4$.

For $\epsilon > 0$, only the points $(\tilde{z}_\pm, 0, \theta_-)$ and $(\tilde{z}_*, u_*, \theta_+)$ persist as equilibria, and only the planes $\theta = \theta_\pm$ remain invariant. Moreover, on the invariant plane U_0, the flow of (2.2) - (2.4) with $0 < \epsilon \ll 1$ is governed by an algebraic Ricatti-equation, which tracks the evolution of 1-D subspaces of the (u, v)-linearized dynamics and which can be put into the normal form for slow-passage through a fold.

Remark 2.2. *The dynamics on the invariant plane U_0 correspond to the dynamics on the blown-up cylinder induced by the linear flow, and the reduced $\tilde{z}, \theta$ system tracks the dynamics of one-dimensional subspaces in the Grassmanian $Gr(2, 1)$ under the linearized flow. Here, when $\epsilon = 0$, equilibria of the projectivized flow, determined by the $\tilde{z}$-equation, are given by spatial eigenvalues ν of the (u, v)-linearization about the origin determined by the linear dispersion relation (1.6).*

In order to study the dynamics on U_0 and those of the full system (2.2) - (2.4), we make one further simplifying step. In particular, we complete the square $\tilde{z} = z + c/2$, obtaining

$$z_\zeta = -z^2 - \theta + u^2, \tag{2.6}$$
$$u_\zeta = (z + c/2)u, \tag{2.7}$$
$$\theta_\zeta = \epsilon(1 - (\theta + c^2/4)^2). \tag{2.8}$$

We shall work with this system in Sections 2 - 4 to establish the main results for the heteroclinic orbit Γ_ϵ, and prove Theorem 1. In the next subsection, we first study the $\epsilon = 0$ system. Then, in the subsequent subsections, we will analyze the dynamics for $0 < \epsilon \ll 1$ and show that there is a transverse intersection of the unstable manifold of $(z_+, 0, \theta_-)$ and the stable manifold of (z_*, u_*, θ_+), for sufficiently small $\epsilon > 0$. The heteroclinic Γ_ϵ will lie in that intersection, see Figure 2.1 for a depiction.

2.2 The $\epsilon = 0$ dynamics

We next study the $\epsilon = 0$ limit of (2.6) - (2.8). For $\epsilon = 0$, the planes $\{\theta = \text{constant}\}$ are invariant. The phase portraits on these invariant planes are depicted in Figure 2.2. The equilibria are now represented by

$$(z_\pm(\theta), u) = (\pm\sqrt{-\theta}, 0), \quad \theta \leq 0; \qquad (z_*, u_*(\theta)) = (-c/2, \sqrt{\theta + c^2/4}), \qquad \theta > -c^2/4.$$

The equilibria $(z_+, 0, \theta)$ are stable in the z-direction for all $\theta < 0$ and unstable in the u-direction for all $\theta \leq 0$. We let $\tilde{W}^u(z_+, 0, \theta)$ denote the 1-D unstable manifold of $(z_+, 0, \theta)$. The equilibria $(z_-, 0)$ are unstable in the z-direction for all $\theta < 0$. Then, in the u-direction, they are stable for $\theta < -c^2/4$ and unstable for $\theta \in (-c^2/4, 0]$. Finally, the other equilibria (z_*, u_*, θ) of (2.6)-(2.8) with $\epsilon = 0$ have one-dimensional stable manifolds, $\tilde{W}^s(z_*, u_*, \theta)$. The bounded portions of these manifolds converge in backward time for $\theta \leq 0$ to the equilibrium $(z_-, 0, \theta)$ (as may be seen from a null-cline analysis).

With θ as a parameter, the (z, u)-vector-field has Jacobian
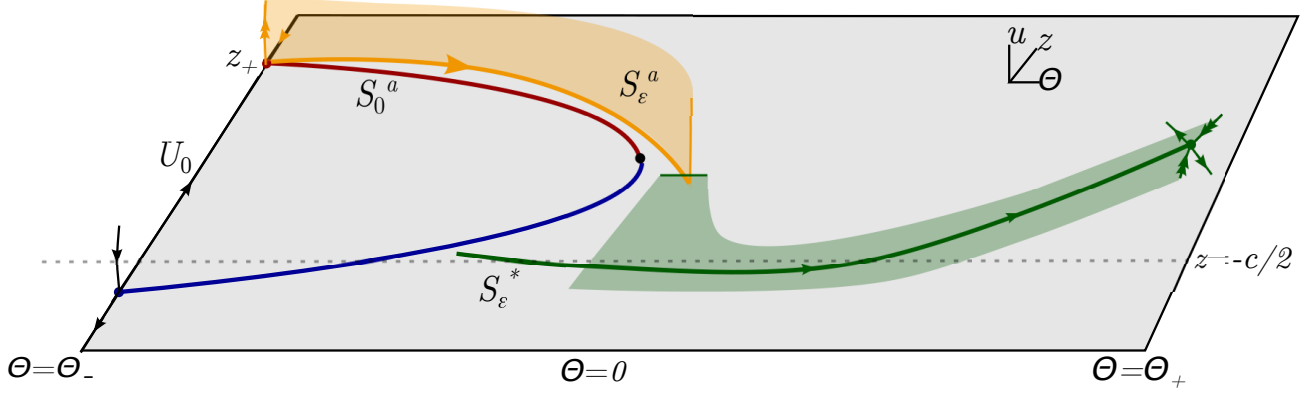
$$\begin{pmatrix} -2z & 2u \\ u & z + c/2 \end{pmatrix}.$$

Figure 2.1: Phase portrait for (2.6)-(2.8) for $0 < \epsilon \ll 1$. Red and blue curves give the critical attracting and repelling sets $S_0^{a/r}$, contained in the invariant plane $\{u = 0\}$ (black), which make up the fold curve for $\epsilon = 0$. S_ϵ^a, depicted in orange, gives the perturbed slow manifold for $\epsilon > 0$. Green curve gives the perturbed slow manifold for the $\epsilon = 0$ equilibrium curve (z_*, u_*, θ). Unstable manifold $W^u(z_+, 0, \theta_-)$ in orange foliated over S_ϵ^a, stable manifold $W^s(z_*, u_*, \theta_+)$, each two-dimensional with one slow dimension and one fast dimension.
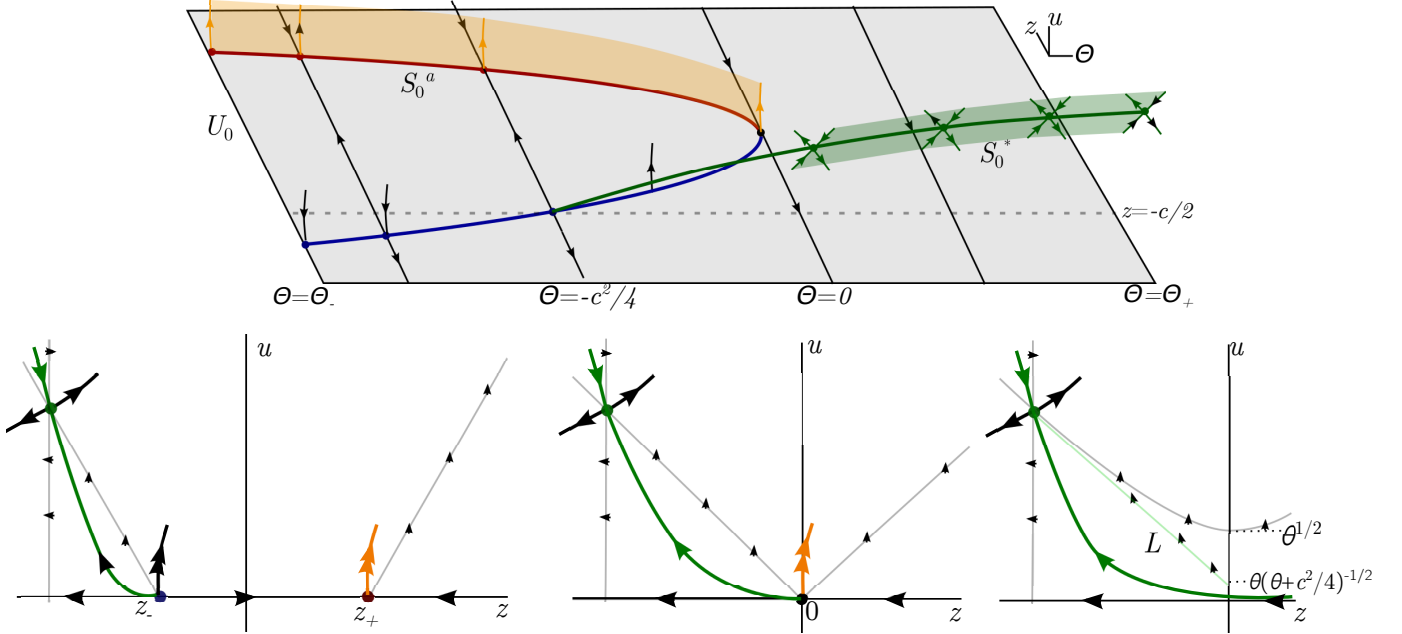

Figure 2.2: Top: Phase portrait for (2.6)-(2.8) for $\epsilon = 0$. Each point $(z_+, 0, \theta)$ on S_0^a has one-dimensional unstable manifold $\tilde{W}^u(z_+, 0, \theta)$ (orange fibers), while each point (z_*, u_*, θ) on S_0^* has a one-dimensional stable manifold $\tilde{W}^s(z_*, u_*, \theta)$ (green fibers). Bottom: (z, u) phase portraits for fixed θ and $\epsilon = 0$ in the cases $-c^2/4 < \theta < 0, \theta = 0$, and $\theta > 0$ from left to right. Light grey lines depict nullclines. The green curves denote $\tilde{W}^s(z_*, u_*, \theta)$. In the bottom right figure, the trapping line L defined in (2.13) is depicted in light green.

At the equilibrium $(z_+, 0) = (\sqrt{-\theta}, 0)$, the Jacobian has the following eigenvalue and eigenvector pairs:

$$\nu = -2z_+, V = (1, 0)^T, \qquad \nu = z_+ + c/2, V = (0, 1)^T.$$

Hence, it is a saddle for each $\theta < 0$, and the local unstable manifold is given as

$$\tilde{W}^u(z_+, 0, \theta) := \{(z, u) \, : \, z = h^u(u; \theta)\} \tag{2.9}$$

$$h^u(u; \theta) = z_+ + \frac{u^2}{4z_+ + c} - \frac{3u^4}{2(3z_+ + c)(4z_+ + c)^2} + \mathcal{O}(|u|^6), \tag{2.10}$$

while its stable manifold is simply a subset of the z-axis. At the equilibrium $(z_-, 0) = (-\sqrt{-\theta}, 0)$, the Jacobian has eigenvalue and eigenvector pairs

$$\nu = -2z_-, V = (1, 0)^T, \qquad \nu = (z_- + c/2), V = (0, 1)^T.$$

11

Hence, the equilibrium is a saddle for $\theta < -c^2/4$ and a source for $-c^2/4 < \theta < 0$. We remark that for $-c^2/36 < \theta < 0$ the direction $(1,0)^T$ is the weak unstable direction and $(0,1)^T$ is the strong unstable direction, while these roles are reversed for $\theta < -c^2/36$. In the former case, we can conclude that in backwards time, $\tilde{W}^s(z_*, u_*, \theta)$ approaches the equilibrium $(z_-, 0)$ tangentially along the z-axis (see Fig. 2.2, bottom left frame). Similar analysis can be done to obtain the expansion for the strong unstable manifold in the u-direction but, as it is not needed for this analysis, we omit it.

Finally, at the equilibrium (z_*, u_*), the Jacobian has the following eigenvalue and eigenvector pairs:

$$\nu_{*,\pm} = c/2 \pm \sqrt{3c^2/4 + 2\theta}, \qquad V_\pm = \left(\frac{\nu_{*,\pm}}{\sqrt{\theta + c^2/4}}, 1 \right)^T.$$

Hence, it is a saddle. The local stable manifold is given by a graph over the z-coordinate as

$$\tilde{W}^s(z_*, u_*, \theta) := \{(z, u) \ : \ u = h^s(z; \theta)\} \tag{2.11}$$

$$h^s(z; \theta) = u_* + b_1(z - z_*) + b_2(z - z_*)^2 + b_3(z - z_*)^3 + \mathcal{O}(|z - z_*|^4)$$

$$b_1 = \frac{-c - (3c^2 + 8\theta)^{1/2}}{2\sqrt{c^2 + 4\theta}}, \quad b_2 = \frac{(c + (3c^2 + 8\theta)^{1/2})(c(3c^2 + 8\theta)^{1/2} - 2(c^2 + 6\theta))}{2(c^2 + 4\theta)^{3/2}(c - 3(3c^2 + 8\theta)^{1/2}},$$

$$b_3 = \frac{c(c + (3c^2 + 8\theta)^{1/2})\left(-2(c^2 + 6\theta) + c(3c^2 + 8\theta)^{1/2}\right)\left(4(2c^2 + 7\theta) + c(3c^2 + 8\theta)^{1/2}\right)}{(c^2 + 4\theta)^{5/2}(c - 3(3c^2 + 8\theta)^{1/2})^2(c - 2(3c^2 + 8\theta)^{1/2})}.$$

$$\tag{2.12}$$

Using these facts with a standard nullcline analysis, one obtains the phase portraits in Figure 2.2. From this analysis and a trapping region argument, one can directly see that for each $\theta > 0$ small the stable manifold $\tilde{W}^s(z_*, u_*, \theta)$ intersects the u-axis at a point u with $0 < u < \sqrt{\theta}$. It turns out we can obtain better control of this intersection point. This is the subject of the following lemma:

Lemma 2.1. *For each $\theta > 0$ sufficiently small, $\tilde{W}^s(z_*, u_*, \theta)$ intersects the set $\{z = 0\}$ transversely at one point $(0, u_s(\theta))$ with*

$$0 < u_s(\theta) \leq \frac{\theta}{\sqrt{\theta + c^2/4}}.$$

Proof. We construct a trapping region for $\tilde{W}^s(z_*, u_*, \theta)$, flowed backwards in ζ. Let

$$L := \{(z, u) \,|\, u = u_* + m(z - z_*), z \in (z_*, 0]\}, \quad m := -\frac{c}{2\sqrt{\theta + c^2/4}}, \tag{2.13}$$

where m is the slope of the z-nullcline at (z_*, u_*). We find $L \cap \{z = 0, u \in (0, \sqrt{\theta})\} \neq \varnothing$ for all $\theta > 0$ since

$$u_* - m z_* = \sqrt{\theta + c^2/4} - \frac{c^2}{4\sqrt{\theta + c^2/4}} = \frac{\theta}{\sqrt{\theta + c^2/4}} > 0$$

Next, one can readily calculate that on L

$$\frac{u_\zeta}{z_\zeta} - m = \frac{1}{\sqrt{1 + 4\theta/c^2}} + \frac{\sqrt{c^2 + 4\theta}(2cz - 4\theta)}{4\theta(c + 2z)} < 0,$$

for all $z \in (-c/2, 0)$ and any $\theta > 0$ sufficiently small. Hence, the flow points "outwards" along L in forward time. This shows that the slope of the vector field along L is more negative than that of the line L itself, and hence that the flow points outward along L. Combining this with the facts that the flow also points outward along the u-nullcline at $z = -c/2$ and that the $u = 0$ line is invariant, we obtain that $\tilde{W}^s(z_*, u_*, \theta)$ must intersect $I := \{(0, u) \,|\, 0 < u < \sqrt{\theta}\}$ with $u < \theta/\sqrt{\theta + c^2/4}$. Finally, transversality follows by the properties of the vector field along the line I. $\qquad \square$

Since L defines a boundary of the trapping region in the above proof, we also have the following corollary:

Corollary 2.2. *Let $\delta > 0$ be small, fixed, and independent of ϵ. There exist a $\theta_0 > 0$ sufficiently small and a constant $C_\delta > 0$, possibly dependent on δ, such that the intersection point $(\delta, u_{s,\delta}(\theta)) := \tilde{W}^s(z_*, u_*, \theta) \cap \{z = -\delta\}$ satisfies*

$$0 < u_{s,\delta}(\theta) \leq C_\delta \theta, \tag{2.14}$$

uniformly for all $\theta \in (0, \theta_0)$.

3   Invariant manifolds, foliations, and slow flow

In this section, we analyze the dynamics of system (2.6)–(2.8) for $0 < \epsilon \ll 1$. Our goal will be to use geometric singular perturbation theory [12, 23] to view $W^{\mathrm{u}}(z_+, 0, \theta_-)$ as a perturbation of the union of $\epsilon = 0$ manifolds $\cup_{\theta \in (-1 - c^2/4, 0]} \tilde{W}^{\mathrm{u}}(z_+, 0, \theta)$ and $W^{\mathrm{s}}(z_*, u_*, \theta_+)$ as a perturbation of the union of $\epsilon = 0$ manifolds $\cup_{\theta \in (-c^2/4, 1 - c^2/4]} \tilde{W}^{\mathrm{s}}(z_*, u_*, \theta)$.

Slow passage through a fold   Let us begin with $W^{\mathrm{u}}(z_+, 0, \theta_-)$. First, for $\epsilon = 0$ the curve of equilibria

$$S_0^a := \{(z, u, \theta) \ : \ z = z_+(\theta), u = 0, \theta \in [-1 - c^2/4, 0)\}$$

is a normally hyperbolic invariant manifold with expanding direction in the u direction and attracting direction in the z direction for all $\theta \leq -b$, for some $b > 0$ fixed, small, and independent of ϵ. Note that this family collides with a repelling curve of equilibria $S_0^r := \{z = z_-(\theta), u = 0, \theta \in [-1 - c^2/4, 0)\}$ in a generic fold bifurcation at $\theta = 0$, and hence loses normal hyperbolicity at $\theta = 0$.

Applying Fenichel theory to the dynamics on the invariant set $U_0 = \{u = 0\}$, that is to the fast-slow subsystem on the invariant (z, θ)-plane, we see that the critical manifold S_0^a perturbs smoothly in $0 < \epsilon \ll 1$ to a 1-D invariant slow manifold $S_\epsilon^a \subset U_0$ for $\theta < -b < 0$. Also note that S_ϵ^a makes up the weak unstable manifold of the left equilibrium $(z_+, 0, \theta_-)$. Since $\theta_\zeta \approx \epsilon$ near $\theta = 0$, Theorem 2.1 of [28] allows one to track S_ϵ^a forward in $\theta \geq -b$ past the fold point at the origin. Further, one can rigorously calculate the bifurcation delay in $\theta > 0$. In particular, setting

$$\tilde{\Sigma}_\delta := \{(z, \theta) \ : \ z = -\delta, \theta \in (0, \delta)\},$$

one can adapt Theorem 2.1 [28] to obtain the following result for the fast-slow subsystem on U_0:

Proposition 3.1. *Let $\delta > 0$ be fixed small. There exists an $\epsilon_0 > 0$ such that, for all $0 < \epsilon \leq \epsilon_0$, the slow invariant manifold S_ϵ^a passes through the section $\tilde{\Sigma}_\delta$ at a point $(z, \theta) = (-\delta, \theta_a(\epsilon))$ with*

$$\theta_a(\epsilon) = \Omega_0 \left(1 - \frac{c^4}{16} \right)^{2/3} \epsilon^{2/3} + \mathcal{O}(\epsilon \ln(\epsilon)), \tag{3.1}$$

where Ω_0 is the smallest positive zero of $J_{-1/3}(2z^{3/2}/3) + J_{1/3}(2z^{3/2}/3)$ and $J_{\pm 1/3}$ are Bessel functions of the first kind. (Note z is a generic complex variable here, distinct from z introduced in (2.6) -(2.8), and also $\Omega_0 = 2.338107...$)

Proof. Define the following change of coordinates

$$z = -(1 - c^4/16)^{1/3} \tilde{x}, \qquad \theta = -\left(1 - \frac{c^4}{16} \right)^{2/3} \tilde{y}, \qquad \zeta = \tau \left(1 - \frac{c^4}{16} \right)^{-1/3}.$$

On the invariant set U_0, the system (2.6)–(2.8) then takes the form

$$\frac{d\tilde{x}}{d\tau} = \tilde{x}^2 - \tilde{y}, \tag{3.2}$$

$$\frac{d\tilde{y}}{d\tau} = \epsilon \left(-1 - \frac{c^2}{2(1 - \frac{c^4}{16})^{1/3}} \tilde{y} + (1 - \frac{c^4}{16})^{1/3} \tilde{y}^2 \right).$$

This system is equivalent to equation (2.5) in [28] with their g defined as $g(\tilde{x}, \tilde{y}, \epsilon) = \left(-1 - \frac{c^2}{2(1 - \frac{c^4}{16})^{1/3}} \tilde{y} + (1 - \frac{c^4}{16})^{1/3} \tilde{y}^2 \right)$.

Hence, Theorem 2.1 in [28] shows that $\tilde{y} = -\Omega_0 \epsilon^{2/3} + \mathcal{O}(\epsilon \ln(\epsilon))$ on $\tilde{\Sigma}_\delta$. Translating this back, one obtains $\theta_a(\epsilon)$, and the result is established. $\square$

Next, notice that the subset

$$U_0^r := \{(z, u, \theta) \ : \ z > -c/2, u = 0\},$$

of the invariant plane U_0, is a normally hyperbolic (repelling) invariant manifold for all $\epsilon \geq 0$ (for completeness we also notice that the corresponding subset $U_0^a \subset U_0$ with $z < -c/2$ is normally attracting). The dynamics in the normal direction to U_0^r are exponentially repelling, while the dynamics in the tangential directions along U_0^r are exponentially attracting in a neighborhood of S_0^a. Hence, the dynamics in a tubular neighborhood of S_0^a

are smoothly foliated by 1-D unstable fibers which we denote by $\mathcal{F}^{\mathrm{uu}}_{(z,\theta)}$. The Fenichel theory [12, 23] guarantees that these fibers can be written as a graph over the normal direction

$$\mathcal{F}^{\mathrm{uu}}_{(z,\theta)} := \{(z, u, \theta) \,|\, (z, \theta) = h^{\mathrm{uu}}(u; z, \theta), |u| \le \gamma\},$$

for some $\gamma > 0$ small and independent of ϵ. Here, h^{uu} is C^r-smooth in u, C^{r-1}-smooth in the base-point (z, θ) for any $r \in \mathbb{N}$, and satisfies

$$h^{\mathrm{uu}}(0; z, \theta) = (z, \theta), \quad \frac{d}{du} h^{\mathrm{uu}}(0; z, \theta) = 0.$$

This foliation satisfies the invariance condition

$$\Phi_\zeta(\mathcal{F}^{\mathrm{uu}}_{(z,\theta)}) \subset \mathcal{F}^{\mathrm{uu}}_{\phi_\zeta(z,\theta)},$$

where Φ_ζ is the flow of the full 3-D system, and ϕ_ζ is the flow on the invariant set U_0. For the base points on S_0^a in particular, these fibers are given by the unstable manifolds $\tilde{W}^{\mathrm{u}}(z_+, 0, \theta)$. This foliation persists smoothly for $0 < \epsilon \ll 1$, but we suppress the ϵ-dependence to simplify notation.

For base points on the perturbed slow manifold S_ϵ^a, the union of fibers gives a local representation of the unstable manifold of the point $(z_+, 0, \theta_-)$, and $\mathcal{F}^{\mathrm{uu}}_{(z_+,\theta_-)}$ gives its local strong unstable manifold,

$$W^{\mathrm{u}}(z_+, 0, \theta_-) \cap \{|u| \le \gamma\} = \bigcup_{(z,\theta) \in S_\epsilon^a} \mathcal{F}^{\mathrm{uu}}_{(z,\theta)},$$

for some $\gamma > 0$ sufficiently small. See Figure 2.1 for a depiction. In addition, such a smooth foliation also holds in a neighborhood of the origin $(z, u, \theta) = (0, 0, 0)$, since the dynamics in z are weakly exponential for $-1 \ll \theta < 0$ and algebraic for $\theta \ge 0$.

As we are interested in how the manifold $W^{\mathrm{u}}(z_+, 0, \theta_-)$ behaves in a neighborhood of the origin, we extend the section $\tilde{\Sigma}_\delta$ into the u-direction, defining for $\delta, \eta, \gamma > 0$ fixed small,

$$\Sigma_\delta := \{(z, \theta, u) \,:\, z = -\delta, \theta \in (-\eta, \eta), u \in [0, \gamma)\}.$$

We can now use the strong-unstable fibers over S_ϵ^a to describe the intersection of $W^{\mathrm{u}}(z_+, 0, \theta_-)$ with Σ_δ.

Lemma 3.2. *Fix $\delta, \eta, \gamma > 0$ small. Then there exists an ϵ_0 such that for all $\epsilon \in [0, \epsilon_0)$ the unstable manifold $W^{\mathrm{u}}(z_+, 0, \theta_-)$ intersects Σ_δ transversely and is a graph in θ of a smooth function $g^u : \mathbb{R} \to \mathbb{R}$ over the u-coordinate:*

$$W^{\mathrm{u}}(z_+, 0, \theta_-) \cap \Sigma_\delta = \{(-\delta, u, g^u(u; \epsilon)) \,,\, u \in [0, \gamma)\}.$$

Proof. This follows by the transverse intersection of S_ϵ^a with $\tilde{\Sigma}_\delta$, the fact that the fibers $\mathcal{F}^{\mathrm{uu}}_{(z,\theta)}$ are vertical at leading order in u, and the smoothness of the fibers $\mathcal{F}^{\mathrm{uu}}_{(z,\theta)}$. $\square$

Next, we use Fenichel theory to conclude that, for $0 < \epsilon \ll 1$, the manifold $W^{\mathrm{s}}(z_*, u_*, \theta_+)$ is a smooth perturbation of the union of stable manifolds $\cup_{\theta > -c^2/4} \tilde{W}^{\mathrm{s}}(z_*, u_*, \theta)$ for $\epsilon = 0$. Indeed the saddle curve

$$S_0^* := \{(z, u, \theta) = (z_*, u_*, \theta) \,:\, \theta \in (-c^2/4, 1 - c^2/4)\},$$

depicted in green in Figure 2.2, persists for $0 < \epsilon \ll 1$ as a 1-D normally hyperbolic invariant slow manifold S_ϵ^*. The asymptotic expansion of S_ϵ^* is given by

$$z = -\frac{c}{2} + \epsilon \frac{1 - \left(\theta + \frac{c^2}{4}\right)^2}{2\left(\theta + \frac{c^2}{4}\right)} + \mathcal{O}(\epsilon^2), \qquad u = \sqrt{\theta + \frac{c^2}{4}} - \epsilon \frac{c}{4} \frac{1 - \left(\theta + \frac{c^2}{4}\right)^2}{\left(\theta + \frac{c^2}{4}\right)^{3/2}} + \mathcal{O}(\epsilon^2). \tag{3.3}$$

We have

Lemma 3.3. *Fix $\delta, \eta, \gamma > 0$ small. There exists an $\epsilon_0 > 0$ such that, for all $\epsilon \in (0, \epsilon_0)$, the invariant manifold $W^{\mathrm{s}}(z_*, u_*, \theta_+)$ intersects the section Σ_δ transversely in a curve which is described as the graph $g^{\mathrm{s}} : \mathbb{R} \to \mathbb{R}$ over the θ coordinate:*

$$W^{\mathrm{s}}(z_*, u_*, \theta_+) \cap \Sigma_\delta = \{(-\delta, g^{\mathrm{s}}(\theta; \epsilon), \theta)\}, \qquad g^{\mathrm{s}}(\theta; \epsilon) = \mathcal{O}(\epsilon + \theta). \tag{3.4}$$

14

Proof. For $\epsilon = 0$, existence, transversality, as well the bound $|g^{\mathrm{s}}(\theta)| \leq C\theta$ for some C independent of ϵ, follow by Lemma 2.1 and smooth dependence of $\tilde{W}^{\mathrm{s}}(z_*, u_*, \theta)$ on θ. Then, for $0 < \epsilon \ll 1$, Fenichel theory implies that the curve S_0^* of saddle equilibria (z_*, u_*, θ) for $\epsilon = 0$ perturbs to a slow, normally hyperbolic invariant manifold for $0 < \epsilon \ll 1$ which forms the weak stable manifold of (z_*, u_*, θ_+). Also by the Fenichel theory, the manifolds $\tilde{W}^{\mathrm{s}}(z_*, u_*, \theta)$ perturb to the strong-stable fibers of $W^{\mathrm{s}}(z_*, u_*, \theta_+)$. The result then follows by smooth dependence on ϵ. $\qquad\square$

From these two results, since the curve $W^{\mathrm{u}}(z_+, 0, \theta_-) \cap \Sigma_\delta$ is a graph over u and is vertical at leading order and the curve $W^{\mathrm{s}}(z_*, u_*, \theta_+) \cap \Sigma_\delta$ is a graph over θ, one generically expects the desired intersection to exist for sufficiently small ϵ; see Figure 3.1. We demonstrate this in the next section. Furthermore, the bifurcation delay prediction for θ can then be translated to a μ-prediction for the delay

$$\mu_{\mathrm{fr}} \approx c^2/4 + \theta_a(\epsilon),$$
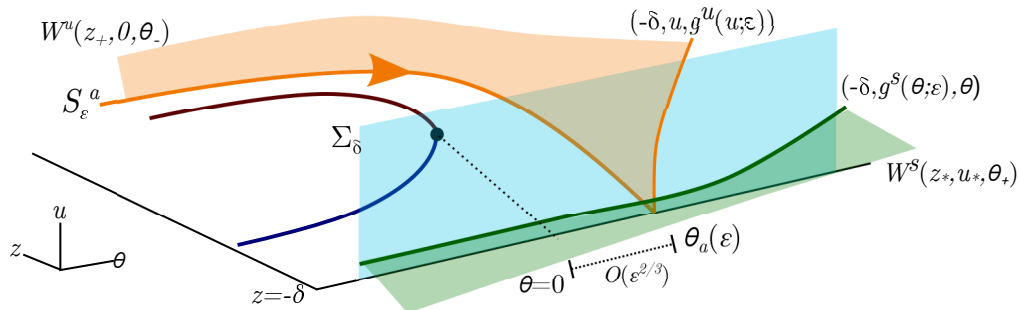
recall (3.1), which will then establish (1.14).

Figure 3.1: Dynamics near the origin, depicting the intersection of $W^{\mathrm{u}}(z_+, 0, \theta_-)$ (orange) and $W^{\mathrm{s}}(z_*, u_*, \theta_+)$ (green) with the section Σ_δ (light blue) and how the transverse intersection is obtained. Intersections with Σ_δ are depicted as solid lines (orange and green respectively) without arrows. Red and blue curves once again depict the $\epsilon = 0$ fold curve $S_0^a \cup S_0^r$.

Remark 3.1. *For each fixed value of $c \in (0, 2)$, Proposition 3.1 is an asymptotic result valid for sufficiently small values of ϵ. Here, we observe that the opposite limit in which $\epsilon > 0$ is fixed and $c \to 2^-$ is a different singular limit. First, with $\epsilon > 0$ fixed, there is no asymptotic time scale separation in the system (1.13)-(1.15) on $\{u = 0\}$ for the variables z and θ. More importantly, with $c = 2$, the system has a fixed point at $(z, \theta) = (0, 0)$, and solutions with initial data in that region of the fourth quadrant between the parabola $\theta = -z^2$ and the positive z-axis approach that fixed point, i.e., $\theta(\zeta) \leq 0$ for all ζ. In contrast, for any value of $c < 2$, no matter how close to 2, the origin is no longer a fixed point, and solutions with initial data in the same region approach the invariant line $\{\theta = 1 - \frac{c^2}{4}\}$ with $z \to -\infty$. Hence, the limit $c \to 2^-$ is a different singular limit. In a manner similar to [15], we expect the absolute spectrum to once again play a role in determining the value of θ on exit from a neighborhood of the origin, and hence the location of the front interface for fixed $\epsilon > 0$. We do not address this here, since our interest in the quenching problem is for small ϵ.*

4   Dynamics near origin: completing the proof of Theorem 1

To construct the desired intersection, we use the foliation graph h^{uu} of U_0 to straighten the fibers, and decouple the (z, θ)-dynamics from the u dynamics. In these new coordinates, the unstable manifold $W^{\mathrm{u}}(z_+, 0, \theta_-)$ is vertical, while $W^{\mathrm{s}}(z_*, u_*, \theta_+)$ still intersects Σ_δ in a graph over θ. To begin, we use the hyperbolic dynamics normal to $U_0^r = \{u = 0, z > -c/2\}$ to straighten the fibers in a neighborhood of U_0^r so that the z and θ equations become independent of u. In particular, the function h^{uu}, which defines the strong-unstable foliation of U_0^r, defines a smooth coordinate change

$$(z_1, \theta_1) = h^{\mathrm{uu}}(u; z, \theta), \ u_1 = u.$$

Here, we have that $h^{\mathrm{uu}}(u; z, \theta) = I_2 + \tilde{h}^{\mathrm{uu}}(u; z, \theta)$ with $\tilde{h}^{\mathrm{uu}}(u; z, \theta) = \mathcal{O}(u^2)$ uniformly in z, θ, and ϵ, and hence is locally invertible for $|u| < \gamma$.

By substituting $(z, \theta) = (h^{uu})^{-1}(z_1, \theta_1)$ and $u = u_1$ into (2.6)–(2.8) and using the invariance property , we obtain the following system:

$$z_{1,\zeta} = -z_1^2 - \theta_1, \tag{4.1}$$

$$u_{1,\zeta} = u_1 f_1(z_1, \theta_1, u_1; \epsilon), \tag{4.2}$$

$$\theta_{1,\zeta} = \epsilon f_2(z_1, \theta_1, u_1; \epsilon) \tag{4.3}$$

for smooth functions f_1, f_2 with

$$f_1(z_1, \theta_1, 0; \epsilon) = z_1 + c/2, \qquad f_2(z_1, \theta_1, 0; \epsilon) = 1 - (\theta_1 + c^2/4)^2,$$

and $f_i(z_1, \theta_1, u; \epsilon) - f_i(z_1, \theta_1, 0; \epsilon) = O(u^2)$ as $u \to 0$. Note the dynamics on U_0^r are left unchanged. In a neighborhood of U_0^r, the manifolds $W^u(z_{1,+}, 0, \theta_{1,-})$ and $W^s(z_{1,*}, u_{1,*}, \theta_{1,+})$ can be described by the dynamics of the base points in U_0^r of the fibers which they intersect.

Next, in view of Lemma 3.2, the unstable manifold is now vertical,

$$W^u(z_+, 0, \theta_-) = \bigcup_{(z_1, \theta_1) \in S_\epsilon^a} \{(z_1, u_1, \theta_1) \ : \ |u_1| \leq \gamma\}.$$

Thus, in (4.1)-(4.3),

$$W^u(z_+, 0, \theta_-) \cap \Sigma_\delta = \{(-\delta, u, \theta_a(\epsilon)) \ : \ |u| \leq \gamma\}, \tag{4.4}$$

where we recall that $\theta_a(\epsilon)$ is the intersection of S_ϵ^a with $z_1 = -\delta$ defined in (3.1) (and which is unchanged in these new coordinates since $u = 0$).

Furthermore, in view of Lemma 3.3, we can also conclude that in the new coordinates

$$W^s(z_*, u_*, \theta_+) \cap \Sigma_\delta = \{(-\delta, \tilde{g}^s(\theta; \epsilon), \theta)\}, \tag{4.5}$$

with $|\tilde{g}^s(\theta; \epsilon)| \leq C(\theta + \epsilon)$, since the fibers $\mathcal{F}^{uu}$ vary quadratically in u. Hence, we seek intersections of the curves described in (4.4) and (4.5). Equating the two curves, we obtain the matching equations

$$u = \tilde{g}^s(\theta; \epsilon), \tag{4.6}$$

$$\theta_a(\epsilon) = \theta, \tag{4.7}$$

where u and θ are free in $(-\gamma, \gamma)$ and $[0, \eta)$, respectively. Hence, for any $\epsilon \in (0, \epsilon_0)$, we choose $\theta = \theta_a(\epsilon)$ and $u = \tilde{g}^s(\theta_a(\epsilon); \epsilon)$, to conclude the desired intersection. We note that at the intersection location $\theta_a(\epsilon)$ the u coordinate is $\mathcal{O}(\epsilon^{2/3})$. A standard finite-time argument shows that the additional delay in θ needed for $u(\zeta) = \sqrt{\mu_c}/2 = c/4$ is then $o(\epsilon^{2/3})$ and thus higher-order. This completes the proof of the theorem.

5 Stationary fronts: geometric desingularization analysis

In this section, we begin the proof of Theorem 2. That is we study fronts created by a stationary quench, which solve (1.3)-(1.4) with $c = 0$,

$$u_\xi = v, \tag{5.1}$$

$$v_\xi = -\mu u + u^3, \tag{5.2}$$

$$\mu_\xi = -\epsilon(1 - \mu^2), \qquad \mu(0) = 0. \tag{5.3}$$

Here, $\xi = x - ct$ reduces to $\xi = x$. We first note system (5.1)-(5.3) is invariant under the reflection (u, v, μ) to $(-u, -v, \mu)$. We then note that for $\epsilon = 0$, the system (5.1)-(5.3) has normally hyperbolic manifolds which are curves of saddle equilibria

$$S_0^\pm = \{(u, v, \mu) = (\pm\sqrt{\mu}, 0, \mu), \mu > \tilde{\eta}\} \tag{5.4}$$

$$S_0^0 = \{(u, v, \mu) = (0, 0, \mu), \mu < -\tilde{\eta}\}, \tag{5.5}$$

where $\tilde{\eta} > 0$ is small and independent of ϵ. We examine these critical manifolds for $\epsilon = 0$, as well as the perturbed slow manifolds which exist for $0 < \epsilon \ll 1$ by Fenichel theory, in the four-dimensional extended system

$$u_\xi = v \tag{5.6}$$

$$v_\xi = -\mu u + u^3 \tag{5.7}$$

$$\mu_\xi = -\epsilon(1 - \mu^2) \tag{5.8}$$

$$\epsilon_\xi = 0. \tag{5.9}$$

We denote the family of such perturbed slow manifolds as $S_\epsilon^\pm$ and S_ϵ^0 and the union of them for $\epsilon \geq 0$ small as $M^\pm$ and M^0. These correspond to center-like manifolds in the extended system. As mentioned above, for each ϵ-slice, $S_\epsilon^\pm$ forms part of the unstable manifold of the equilibria $(u, v, \mu) = (\pm 1, 0, 1)$ while S_ϵ^0 forms part of the unstable manifold $W^u(0, 0, 1)$ for $\mu > \tilde{\eta}$ and part of the stable manifold $W^s(0, 0, -1)$ for $\mu < -\tilde{\eta}$. These manifolds give the base points of fibers which foliate the manifolds they live in. For example S_ϵ^+ serves as the base points of strong stable/unstable fibers which foliate $W^{s/u}(1, 0, 1)$. Hence, we wish to use the slow manifolds to track the containing invariant manifolds and construct the desired heteroclinic intersection.

We wish to track the perturbed slow manifolds through a neighborhood of $(u, v, \mu) = (0, 0, 0)$, where they lose normal hyperbolicity, using the quasi-homogeneous geometric blow up

$$u = r\bar{u}, \quad v = r^2\bar{v}, \quad \mu = r^2\bar{\mu}, \quad \epsilon = r^3\bar{\epsilon}. \tag{5.10}$$

These coordinates blow up the origin $(0, 0, 0, 0)$ into a 3-sphere $S_3 = \{r = 0, \bar{u}^2 + \bar{v}^2 + \bar{\mu}^2 + \bar{\epsilon}^2 = 1\}$, which is invariant under the induced flow. In particular, it is natural to study the dynamics on and near the sphere using the following three charts defined by $\bar{\mu} = 1, \bar{\epsilon} = 1$, and $\bar{\mu} = -1$, respectively:

$$\text{Entry chart } K_1: \quad u = r_1 u_1, v = r_1^2 v_1, \mu = r_1^2, \epsilon = r_1^3 \epsilon_1 \tag{5.11}$$

$$\text{Rescaling chart } K_2: \quad u = r_2 u_2, v = r_2^2 v_2, \mu = r_2^2 \mu_2, \epsilon = r_2^3 \tag{5.12}$$

$$\text{Exit chart } K_3: \quad u = r_3 u_3, v = r_3^2 v_3, \mu = -r_3^2, \epsilon = r_3^3 \epsilon_3. \tag{5.13}$$

Here, x_i denotes the variable $\bar{x} \in \{\bar{u}, \bar{v}, \bar{\mu}, \bar{\epsilon}\}$ in chart K_i. The change of coordinate map κ_{12} between the charts K_1 and K_2, as well the map κ_{23} between K_2 to K_3 are given as

$$\kappa_{12}: \quad u_2 = \epsilon_1^{-1/3} u_1, \quad v_2 = \epsilon_1^{-2/3} v_1, \quad \mu_2 = \epsilon_1^{-2/3}, \quad r_2 = \epsilon_1^{1/3} r_1, \qquad \epsilon_1 > 0 \tag{5.14}$$

$$\kappa_{23}: \quad u_3 = (-\mu_2)^{-1/2} u_2, \quad v_3 = (-\mu_2)^{-1} v_2, \quad \epsilon_3 = (-\mu_2)^{-3/2}, \quad r_3 = r_2(-\mu_2)^{1/2}, \qquad \mu_2 < 0. \tag{5.15}$$

We remark that the second mapping above, κ_{23}, maps into the exit chart where $\bar{\mu} < 0$. We next collect information about the phase portrait near the sphere $\{r = 0\}$ in each coordinate chart, first describing the entry and exit charts K_1, K_3 and then the re-scaling chart K_2.

Entry chart K_1 phase portrait In chart K_1, the governing equations are

$$u_1' = v_1 + \frac{1}{2}\epsilon_1 u_1(1 - r_1^4) \tag{5.16}$$

$$v_1' = -u_1 + u_1^3 + \epsilon_1 v_1(1 - r_1^4) \tag{5.17}$$

$$\epsilon_1' = \frac{3}{2}\epsilon_1^2(1 - r_1^4) \tag{5.18}$$

$$r_1' = -\frac{1}{2}r_1\epsilon_1(1 - r_1^4). \tag{5.19}$$

Here, we recall that K_1 is defined by $\mu_1 = 1$, and we have introduced the new time variable $\xi_1 = r_1\xi$ to desingularize the vector field, with the prime now denoting the derivative with respect to ξ_1. We note that the system is autonomous so that the reparametrization of solutions leaves the trajectories in phase space intact. The system (5.16)-(5.19) has fixed points at $p^- = (-1, 0, 0, r_1)$, $p^0 = (0, 0, 0, r_1)$, and $p^+ = (1, 0, 0, r_1)$ for each $r_1 \geq 0$. These are exactly the points at which the invariant manifolds S_0^-, S_0^0, and S_0^+, respectively, enter the neighborhood of the blown-up singularity. The equilibrium p_+, and indeed each equilibrium in S_0^+, has one-dimensional stable and unstable eigenspaces contained in the (u_1, v_1) plane and two center directions, one in the r_1 direction, tangential along S_0^+, and the other given by the generalized eigenvector $(0, 1, -2/(1 - r_1^4), 0)$ for $r_1 > 0$ and the eigenvector $(0, 1, -2, 0)$ for $r_1 = 0$ (note the former center direction corresponds to the family

17

of equilibria formed by S_0^+). Thus, S_0^+ lies inside of a two-dimensional center manifold $\mathcal{M}^{c,+}$ which, in the original extended system (5.6) - (5.9), corresponds to the family M^+ of slow manifolds for ϵ small. Due to the strong stable and unstable directions in the (u_1, v_1) directions, $\mathcal{M}^{c,+}$ is normally hyperbolic with strong stable and unstable foliations. The union of the strong unstable fibers forms a center-unstable manifold $\mathcal{M}^{cu,+}$ which corresponds to $W^{cu}(1,0,1)$ in the original coordinates. In K_1, $\mathcal{M}^{cu,+}$ contains the set of all bounded solutions as $\xi_1 \to -\infty$.

Furthermore, the hyperplane $\{r_1 = 0\}$ is an invariant set, and on it the dynamics reduce to

$$u_1' = v_1 + \frac{1}{2}\epsilon_1 u_1$$
$$v_1' = -u_1 + u_1^3 + \epsilon_1 v_1$$
$$\epsilon_1' = \frac{3}{2}\epsilon_1^2$$
$$r_1' = 0.$$

Hence, standard center manifold theory directly implies that, when restricted to $\{r_1 = 0\}$, $p^\pm$ have one-dimensional normally hyperbolic center manifolds, $N_1^\pm$. Moreover, these are not unique due to the presence of both hyperbolic repelling and attracting dynamics in the (u_1, v_1) plane. Note also that p^0 has a one-dimensional normally elliptic center manifold given by $(u_1, v_1, \epsilon_1) = (0, 0, \epsilon_1)$.

We focus on p^+ and N_1^+ for the heteroclinic here. By standard center manifold theory, N_1^+ is tangent at p^+ to the center eigendirection spanned by $(0, -1, 2)$. Asymptotically, it is represented by

$$u_1 = 1 - \frac{\epsilon_1^2}{8} - \frac{73}{128}\epsilon_1^4 + \mathcal{O}(\epsilon_1^6)$$
$$v_1 = -\frac{\epsilon_1}{2} - \frac{5}{16}\epsilon_1^3 - \frac{803}{256}\epsilon_1^5 + \mathcal{O}(\epsilon_1^7). \tag{5.20}$$

This follows from applying the invariance condition, and we recall that all center manifolds in the family have the same expansion in powers of small ϵ_1. See Figure 6.1.

Exit Chart K_3   The phase portrait in K_3 near $r = 0$ can be derived in a similar way. The governing equations are

$$u_3' = v_3 - \frac{1}{2}\epsilon_3 u_3(1 - r_3^4) \tag{5.21}$$
$$v_3' = u_3 + u_3^3 - \epsilon_3 v_3(1 - r_3^4) \tag{5.22}$$
$$\epsilon_3' = -\frac{3}{2}\epsilon_3^2(1 - r_3^4) \tag{5.23}$$
$$r_3' = \frac{1}{2}r_3\epsilon_3(1 - r_3^4). \tag{5.24}$$

This system has a curve of equilibria $S_0^0 = \{(0,0,0,r_3), r_3 \geq 0\}$, each of which have strong stable/unstable directions in the (u_3, v_3) plane. S_0^0 also lies inside a two-dimensional center manifold $\mathcal{M}^{c,0}$ tangent to the (ϵ_3, r_3) plane. Here one such center manifold is given by the plane $\{(0, 0, \epsilon_3, r_3) : \epsilon_3, r_3 \geq 0\}$. This manifold is once again normally hyperbolic with one-dimensional strong stable and unstable fibers. The union of stable fibers gives a local description of a center-stable manifold $\mathcal{M}^{cs,0}$ which corresponds locally to $W^{cs}(0, 0, -1)$. Similarly to K_1, the $r_3 = 0$ plane is invariant with the reduced system

$$u_3' = v_3 - \frac{1}{2}\epsilon_3 u_3$$
$$v_3' = u_3 + u_3^3 - \epsilon_3 v_3$$
$$\epsilon_3' = -\frac{3}{2}\epsilon_3^2$$
$$r_3' = 0.$$

Here we find the trivial center manifold N_3^0 given by $(0, 0, \epsilon_3)$ for $\epsilon_3 \geq 0$.

Hence, by tracking manifolds across the rescaling chart, we wish show that the three-dimensional manifolds $\mathcal{M}^{cs,0}$ and $\mathcal{M}^{cu,+}$ have a two-dimensional intersection, with one direction corresponding to variation in ϵ and the other the direction of the flow.

Rescaling Chart K_2   Finally, we work in the rescaling chart K_2 to identify the geometrically unique solution that represents the desired heteroclinic in the blown-up vector field. In K_2, system (5.6)-(5.9) becomes

$$u_2' = v_2 \tag{5.25}$$
$$v_2' = -\mu_2 u_2 + u_2^3 \tag{5.26}$$
$$\mu_2' = -1 + r_2^4 \mu_2^2 \tag{5.27}$$
$$r_2' = 0. \tag{5.28}$$

Here, the prime denotes the derivative with respect to the new time variable $\xi_2 = r_2 \xi$. We focus on the dynamics of this system on the invariant set $\{r_2 = 0\}$, where the system reduces to

$$u_2' = v_2 \tag{5.29}$$
$$v_2' = -\mu_2 u_2 + u_2^3 \tag{5.30}$$
$$\mu_2' = -1 \tag{5.31}$$
$$r_2' = 0. \tag{5.32}$$

Then, by converting the (u_2, v_2) subsystem into a second-order scalar equation, scaling $u_2 = \sqrt{2}\tilde{u}_2$, and recalling that $\mu_\xi = -\epsilon(1 - \mu^2)$ so that $\mu_2 = -\xi_2$ on $\{r_2 = 0\}$, we find that the governing equation on $\{r_2 = 0\}$ is

$$\tilde{u}_2'' = \xi_2 \tilde{u}_2 + 2\tilde{u}_2^3. \tag{5.33}$$

This is precisely the second Painlevé equation (P_{II}), recall (1.17). Note that the scaling used here to derive $\tilde{u}_2(\xi_2)$ is the same as that used in Section 1.3 for $\tilde{u}(\eta)$ and $w(\eta)$ since $r_2 = \epsilon^{1/3}$ in K_2.

Now, as previewed above while deriving the formal asymptotics, the key solution of (5.33) that is of interest here is the Hastings and McLeod solution, w_{HM} of (1.17), which we denote here by $\tilde{u}_2^*(\xi_2)$. It is the unique solution which satisfies the asymptotic boundary conditions

$$\tilde{u}_2^*(\xi_2) \sim \sqrt{-\xi_2/2}, \ \xi_2 \to -\infty, \qquad \tilde{u}_2^*(\xi_2) \sim \mathrm{Ai}(\xi_2), \ \xi_2 \to +\infty,$$

and which decays strictly monotonically. Finally, scaling back to u_2, this yields the unique monotonically decaying solution $u_2^*(\xi_2)$ of (5.29)-(5.32) with the asymptotics

$$u_2^*(\xi_2) \sim \sqrt{-\xi_2} = \sqrt{\mu_2}, \ \xi_2 \to -\infty, \tag{5.34}$$
$$u_2^*(\xi_2) \sim \sqrt{2}\mathrm{Ai}(\xi_2), \ \xi_2 \to +\infty. \tag{5.35}$$

6   Singular heteroclinic connection on the sphere, transversality

On the blow-up sphere, $\{r = 0\}$, the Hastings-Mcleod solution u_2^* represents a heteroclinic solution connecting the equilibria p^+ on the $\bar{\mu} > 0$ hemisphere to the equilibria p^0 in the $\bar{\mu} < 0$ hemisphere. Below, we find that in the charts K_1 and K_3 this unique connecting orbit gives a 1-D center manifold in the $r_j = 0$ invariant subspaces in chart K_j for both $j = 1, 3$. We thus use this heteroclinic orbit to transport the center unstable manifold $\mathcal{M}^{cu,+}$ from K_1 across the sphere to locate an intersection with the center-stable manifold $\mathcal{M}^{cs,0}$ in K_3. To address the non-uniqueness of the center manifolds in K_1 and K_3, we first construct an intersection between the local 3-D center unstable manifold of the equilibrium p^+ which contains the 1-D center manifold $\kappa_{21}^{-1}u_2^*$ in K_1 and the local 3-D center stable manifold of the equilibrium p^0 which contains the 1-D center manifold $\kappa_{23}u_2^*$. We do this in order to flow these invariant manifolds globally across K_2 using the variational dynamics around u_2^*. We then use inclination properties of the flow in each chart to conclude the same transversality and intersection properties for the center unstable/stable manifolds $\mathcal{M}^{cu,+}$, $\mathcal{M}^{cs,0}$.

Using the inverse coordinate change $\kappa_{12}^{-1} : K_2 \to K_1$, given by $u_1 = u_2\mu_2^{-1/2}, v_1 = v_2\mu_2^{-1}, \epsilon_1 = \mu_2^{-3/2}$, and $r_1 = r_2\mu_2^{1/2}$, we can translate the asymptotics of u_2^* into the variables of chart K_1. We find that, when flowed back through the entry chart coordinates K_1, the solution $\kappa_{12}^{-1}u_2^*(\xi_2)$ asymptotically approaches $p^+ = (1, 0, 0, 0)$ as $\xi_1 \to -\infty$, and it lies on a center manifold, N_1^+, of this equilibrium. In fact, the higher order terms in the asymptotic expansion of the Hastings-McLeod solution as $\xi_2 \to -\infty$, given by

$$u_2^*(\xi_2) = \sqrt{-\xi_2}\left(1 + \frac{1}{8\xi_2^3} - \frac{73}{128\xi_2^6} + \frac{10219}{1024\xi_2^9} + \mathcal{O}(\xi_2^{-12})\right), \tag{6.1}$$

(see for example [6, 1], and also [4] for the full trans-series asymptotics) also agree with the higher-order terms in the expansion of N_1^+; recall (5.20).

In a similar manner, using the coordinate change κ_{23}, we can translate the asymptotics of u_2^* as $\xi_2 \to +\infty$, given in (5.35), into the K_3 variables. We find the set $\kappa_{23}u_2^*$ is a 1-D center manifold of the equilibrium p^0 in the $\{r_3 = 0\}$ invariant subspace. Indeed, using the coordinate transform $\xi_2 = -\mu_2 = (\epsilon_3^{2/3})$ the leading order expansion for the Airy functions

$$\text{Ai}(\xi) = \frac{e^{-\frac{2}{3}\xi^{3/2}}}{2\sqrt{\pi}\xi^{1/4}}\left(1 + \mathcal{O}(\xi^{-3/2})\right), \tag{6.2}$$

$$\text{Ai}'(\xi) = -\frac{\xi^{1/4}e^{-\frac{2}{3}\xi^{3/2}}}{2\sqrt{\pi}}\left(1 + \mathcal{O}(\xi^{-3/2})\right), \tag{6.3}$$

we have the following asymptotic description of the trajectory in K_3

$$u_3 = \frac{\exp(-\frac{2}{3}\epsilon_3^{-1})}{\sqrt{2\pi}}\left(\epsilon_3^{1/2} + \mathcal{O}(\epsilon_3^{3/2})\right), \tag{6.4}$$

$$v_3 = -\frac{\sqrt{2}\exp(-\frac{2}{3}\epsilon_3^{-1})}{\sqrt{2\pi}}\left(\epsilon_3^{1/2} + \mathcal{O}(\epsilon_3^{3/2})\right). \tag{6.5}$$

Thus, this trajectory approaches p^0 tangentially along the center direction formed by the ϵ_3-axis.

As described above, the equilibria p^+ and p^0 each have 1-D strong stable and strong unstable subspaces, along with 2-D center spaces. We let $W_1^{cu}(p^+)$ denote the 3-D local center-unstable manifold of p^+ in K_1 which contains $\kappa_{12}^{-1}u_2^*$ and let $W_3^{cs}(p^0)$ be the 3-D local center-stable manifold of p^0 in K_3 which contains $\kappa_{23}u_2^*$. Furthermore, we let $W_2^{cu}(p^+)$ and $W_2^{cs}(p^0)$ denote the above manifolds in the K_2 coordinates. These manifolds can be continued along a neighborhood of the connecting solution u_2^* using the flow of the K_2 dynamics.
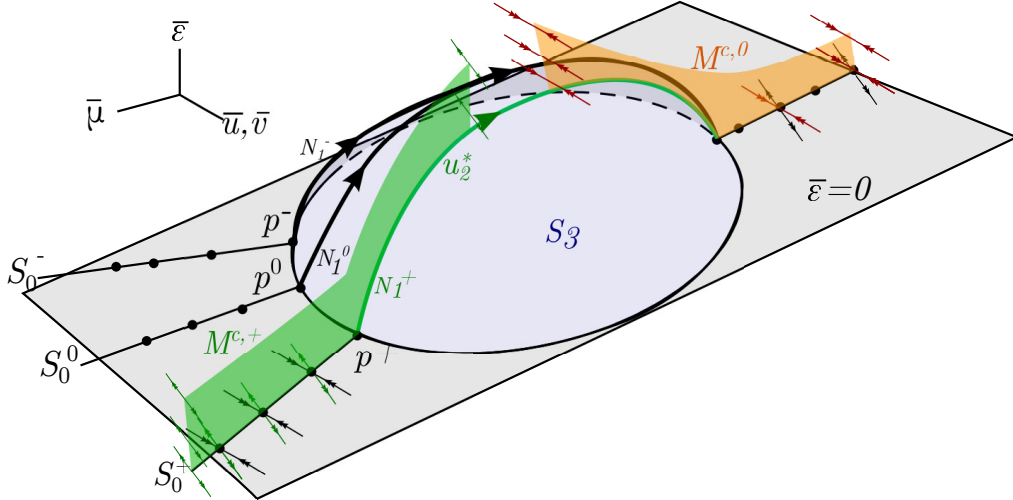

Figure 6.1: Schematic depiction of 4-D blown-up phase space near the blow-up sphere S_3 (light blue) in the coordinates (5.10). The singular heteroclinic u_2^* on S_3 connecting p_+ in chart K_1 to p^0 in chart K_3 is depicted in green. Near the equilibria p_+ this curve also gives the center manifold N_1^+ described in (5.20). Critical equilibria curves $S_0^\pm, S_0^0$ for $r \geq 0$ lying inside the $\bar{\epsilon} = 0$ plane (grey) are given by black lines with dots. The green and orange surfaces respectively denote the 2-D center manifolds $\mathcal{M}^{c,+}$ and $\mathcal{M}^{c,0}$ described in Section 5, and the double-arrowed green and red curves denote 1-D strong unstable and stable fibers. The desired intersection is given for $0 < \epsilon \ll 1$ by the intersection of the union of $\mathcal{M}^{c,+}$ and its strong unstable fibers with $\mathcal{M}^{c,0}$ and its strong stable fibers.

We wish to show that the invariant manifolds $W_1^{cu}(p^+)$ and $W_3^{cs}(p^0)$, globally continued across the sphere intersect transversely with two dimensional intersection containing u_2^*. To do this, we track them both in the rescaling chart K_2 in a neighborhood of u_2^* using the associated variational equation. In particular, letting $U_2^* = (u_2^*, v_2^*, \mu_2^*, 0)^T$, and $F(U)$ denote the 4-D vector-field defined in (5.25) - (5.28), we insert the solution decomposition $U = U_2^* + W$, $W = (w_1, w_2, w_3, w_4)^T \in \mathbb{R}^4$, into the nonlinear system, obtaining

$$W' = A_2(\xi_2)W + G(\xi_2, W), \tag{6.6}$$

$$A_2(\xi_2) = DF(U_2^*(\xi_2)), \qquad G(\xi_2, W) = F(U_2^*(\xi_2) + W) - F(U_2^*(\xi_2)) - DF(U_2^*(\xi_2))W.$$

20

Here A_2 takes the 2x2 block form

$$A_2(\xi_2) = \begin{pmatrix} A_{2,0}(\xi_2) & A_{2,1}(\xi_2) \\ 0_2 & 0_2 \end{pmatrix}, \quad A_{2,0}(\xi_2) = \begin{pmatrix} 0 & 1 \\ \xi_2 + 3(u_2^*)^2 & 0 \end{pmatrix}, \quad A_{2,1}(\xi_2) = \begin{pmatrix} 0 & 0 \\ -u_2^* & 0 \end{pmatrix},$$

where 0_2 denotes the 2x2 zero matrix.

We study the evolution of the tangent spaces of the desired invariant manifolds along u_2^* using the linear variational equation

$$W' = A_2(\xi_2)W. \tag{6.7}$$

Such tangent spaces can be studied using exponential trichotomies [40] to track not only hyperbolic, but also center dynamics about u_2^*. We readily observe that the w_3 and w_4 directions, corresponding to the ϵ_2 and r_2 directions, are constant. Due to the upper diagonal element coupling w_3 to w_2, the subspace spanned by these directions is not invariant. We do note that the w_4 direction is invariant, and spans one dimension of the center bundle. Also, the $w_3 = w_4 = 0$ subspace is invariant and contains the hyperbolic dynamics on both $\mathbb{R}_\pm$. Using the asymptotics of u_2^*, one can obtain the following result

Lemma 6.1. *The system* (6.7) *possesses exponential trichotomies* $\mathbb{R}^4 = E^{s,\pm}(\xi_2) \oplus E^{u,\pm}(\xi_2) \oplus E^{c,\pm}(\xi_2)$ *on both* $\mathbb{R}_\pm$, *with* $E^{s/u,\pm}(\xi_2)$ *contained in the* (w_1, w_2) *subspace and* $(0,0,0,1)^T \in E^{c,\pm}(\xi_2)$ *for all* ξ_2.

Proof. On $\mathbb{R}_+$, the asymptotics of u_2^* given in (5.35) imply that $A_2(\xi_2)$ is a localized perturbation of $\begin{pmatrix} A_{2,Ai}(\xi_2) & 0_2 \\ 0_2 & 0_2 \end{pmatrix}$, where $A_{2,Ai}(\xi_2) = \begin{pmatrix} 0 & 1 \\ \xi_2 & 0 \end{pmatrix}$. As the subsystem $W_h' = A_{2,Ai}(\xi_2)W_h$, $W_h = (w_1, w_2)^T$ is the first-order system formulation of a rescaled Airy equation $w_1'' - \xi_2 w_1 = 0$, it has an exponential dichotomy on $\mathbb{R}_+$ whose stable and unstable subspaces are spanned by the linearly independent functions $w_1 = \text{Ai}(\xi_2)$, $\text{Bi}(\xi_2)$. Standard roughness results then give the existence of an exponential dichotomy on $\mathbb{R}_+$ of the hyperbolic subsystem $W_h' = A_{2,0}(\xi_2)W_h$ of (6.7). Thus, since the coupling term $w_3 u_2^*$ vanishes exponentially fast for $\xi_2 \to +\infty$, such roughness results also give the existence of an exponential trichotomy also for the full system.

On $\mathbb{R}_-$, the hyperbolic subsystem $W_h' = A_{2,0}(\xi_2)W_h$ is an algebraically localized perturbation of another scaled Airy system. In particular, since $u_2^*(\xi_2) \sim \sqrt{-\xi_2}$, we have $A_{2,0}(\xi_2) \sim \begin{pmatrix} 0 & 1 \\ -2\xi_2 & 0 \end{pmatrix}$, so that the corresponding system is approximated by the first order formulation of $w_1'' + 2\xi_2 w_1 = 0$ for $\xi_2 < 0$, which has two linearly independent solutions $w_1 = \text{Ai}(-2^{1/3}\xi_2)$, $\text{Bi}(-2^{1/3}\xi_2)$ that again give the asymptotic stable and unstable space respectively. Roughness once again gives the existence of a dichotomy for the hyperbolic subspaces. The existence of center subspace is obtained by using the fact that w_3 and w_4 are constant, and applying a variation of constants argument to solve the following initial value problem for each w_3-value,

$$W_h' = A_{2,0}(\xi_2)W_h + \begin{pmatrix} 0 \\ u_2^*(\xi_2)w_3 \end{pmatrix}, \qquad W_h(0) = 0, \quad \xi_2 \in \mathbb{R}_-.$$

$\square$

Proposition 6.2. *The 1-D unstable and stable subspaces* $E_2^{u,-}(0)$ *and* $E_2^{s,+}(0)$ *intersect transversely. That is,* $\mathbb{R}^2 = E_2^{u,-}(0) \oplus E_2^{s,+}(0)$.

Proof. It suffices to consider the 2-D hyperbolic subsystem $W_h' = A_{2,0}(\xi_2)W_h$. First, we note this system is the first-order formulation of the linearized Painlevé-II equation

$$0 = L_0 w_1 := w_1'' - (\xi_2 + 3(u_2^*)^2)w_1. \tag{6.8}$$

so that exponentially localized eigenfunctions of the latter correspond to solutions of the former lying in the intersection $E_2^{u,-}(\xi_2) \cap E_2^{s,+}(\xi_2)$. Here L_0 is a L^2 self-adjoint operator, with closed densely-defined domain. This operator takes the form of the often-studied Schrödinger operator $\partial_{\xi_2}^2 + V(\xi_2)$ with potential $V(\xi_2) = -(\xi_2 + 3(u_2^*)^2)$. Since the potential satisfies $|V(\xi_2)| \to +\infty$ as $|\xi_2| \to +\infty$, standard results [34, Thm. XIII.47] give that L_0 has no essential spectrum and the discrete spectrum $\{\lambda_j\}$ satisfies $\lambda_0 \geq \lambda_1 \geq \lambda_2 \geq \dots$ with $\lambda_j \to -\infty$. Such results also give for such operators that if $V(\xi_2) < 0$, the "ground-state" eigenfunction ϕ_0 of the eigenvalue is strictly positive $\phi_0 > 0$. The asymptotics of u_2^* as $|\xi_2| \to \infty$ imply that if our potential has $V(\xi_2) > 0$

at some point then it has $V(\xi_2) > 0$ at most on bounded interval in $\mathbb{R}_-$ and hence, since u_2^* is smooth, that $m = \max_{\xi_2} V(\xi_2)$ is finite. Hence, the potential of the shifted operator $L_0 - (m + \delta)$, for $\delta > 0$ small, is strictly negative. Thus, the ground state eigenfunction is strictly positive.

Now, to obtain a contradiction, assume that the ground-state eigenvalue has $\lambda_0 \geq 0$. Then, differentiating the Painlevé-II equation $u_2'' + (-\xi_2)u_2 - u_2^3 = 0$ in ξ_2, we obtain that

$$L_0 \partial_\xi u_2^* = u_2^*.$$

Also, we recall that $\partial_\xi u_2^* < 0$. We then calculate

$$\lambda_0 \langle \phi_0, \partial_\xi u_2^* \rangle_{L^2} = \langle \phi_0, L_0 \partial_\xi u_2^* \rangle_{L^2} = \langle \phi_0, u_2^* \rangle_{L^2} > 0, \tag{6.9}$$

which is a contradiction because $\partial_\xi u_2^* \cdot \phi_0 < 0$ so that $\langle \phi_0, \partial_\xi u_2^* \rangle_{L^2} < 0$. Hence we have that $\lambda_0 < 0$ and therefore that the hyperbolic subsystem $W_h' = A_{2,0}(\xi_2)W_h$ has no exponentially localized solution and hence the two subspaces in question must intersect trivially. $\square$

Remark 6.1. *We also note that Appendix A gives a rigorous proof of the negativity of the potential, $V(\xi_2) = -(\xi_2 + 3(u_2^*)^2) < 0$, for all ξ_2. This implies that the shift of the operator and results from Schrödinger operators is not needed above. One actually need only study the numerical range $\lambda_0 \|\phi_0\|_{L^2}^2 = \langle L_0 \phi_0, \phi_0 \rangle_{L^2} = -\int_R (\partial_\xi \phi_0)^2 d\xi + \int_R V(\xi) \phi_0^2 d\xi < 0$ to infer the negativity of the ground-state eigenvalue.*

Given the results of Lemma 6.1 and Proposition 6.2 about the linear dynamics around u_2^*, we then can conclude the desired intersection properties of the center-unstable and center-stable manifolds around u_2^*.

Proposition 6.3. *In a tubular neighborhood of u_2^*, the invariant manifolds $W_1^{cu}(p^+)$ and $W_3^{cs}(p^0)$ intersect transversely with two dimensional intersection containing u_2^*.*

Proof. First, we observe that the variational equation (6.6) and the exponential trichotomies on $\mathbb{R}_\pm$ can be used to construct and continue the manifolds $W_1^{cu}(p^+)$ and $W_3^{cs,}(p^0)$ in a neighborhood of u_2^* for all $\mathbb{R}_+$ and $\mathbb{R}_-$ respectively. Furthermore, the tangent spaces of these manifolds along u_2^* are given by the three-dimensional spaces $E_2^{cu,-}(\xi_2) := E_2^{u,-}(\xi_2) \oplus E_2^{c,-}(\xi_2)$ and $E_2^{cs,+}(\xi_2) := E_2^{s,+}(\xi_2) \oplus E_2^{c,+}(\xi_2)$. Restricting to a three-dimensional transverse section $\tilde{\Sigma}_2 = \{\mu_2 = 0\}$, we wish to construct a 1-D family of intersections in $\tilde{\Sigma}_2$ by writing the invariant manifolds locally as graphs over the relevant tangent bundles and constructing a set of matching equations.

In more detail, the transversality given in Proposition 6.2 gives a coordinate basis of $\tilde{\Sigma}_2$ as $\tilde{\Sigma}_2 = E_2^{s,+}(0) \oplus E_2^{u,-}(0) \oplus \text{span}\{e_4\}$, where e_4 points in one of the center directions, while the other center direction points along the flow, transverse to $\tilde{\Sigma}_2$. We let (w_s, w_u, w_4) denote the corresponding coordinates and also note that as these coordinates arise from the nonlinear variation equation, we have that $u_2^*(0) \cap \tilde{\Sigma}$ corresponds to $(w_s, w_u, w_4) = 0$. In these coordinates, we can write the invariant manifolds as graphs

$$W_1^{cu}(p^+) \cap \tilde{\Sigma}_2 = \{(h_-(w_u, w_4), w_u, w_4) : |w_u|, |w_4| \leq \delta\}, h_- : \mathbb{R}^2 \to \mathbb{R}, \tag{6.10}$$

$$W_3^{cs}(p^0) \cap \tilde{\Sigma}_2 = \{(w_s, h_+(w_s, w_4), w_4) : |w_s|, |w_4| \leq \delta\}, h_+ : \mathbb{R}^2 \to \mathbb{R} \tag{6.11}$$

for some $0 < \delta \ll 1$, for smooth functions $h_\pm$ with tangency conditions $h_-(0,0) = D_{w_u,w_4}h_-(0,0) = 0$, and $h_+(0,0) = D_{w_s,w_4}h_+(0,0) = 0$. Intersections of the two invariant manifolds can then be obtained via the following matching equations

$$h_-(w_u, w_4) = w_s, \tag{6.12}$$

$$w_u = h_+(w_s, w_4). \tag{6.13}$$

Note we have equated the w_4 component of each graph description. Rearranging these equations, intersections are then given as zeros of the following set of equations $\mathcal{H}(w_s, w_u; w_4) := (w_s - h_-(w_u, w_4), w_u - h_+(w_s, w_4))^T$. The properties of the graphs then imply

$$\mathcal{H}(0,0;0) = (0,0), \qquad D_{w_s,w_u}\mathcal{H}(0,0;0) = I_2,$$

so that, by the Implicit Function theorem, one can solve for (w_s, w_u) as a function of w_4 near $(0,0,0)$, giving a one-parameter family of solutions parametrized by the w_4 variable, that is r_2, which corresponds to $\bar{\epsilon}$. $\square$

Having constructed the heteroclinic between equilibria on the singular sphere, we now use inclination lemmas to also conclude an intersection between the desired invariant manifolds $\mathcal{M}^{cu,+}$, $\mathcal{M}^{cs,0}$. We state the argument in detail for the dynamics near K_1, and outline the argument for K_3 as it follows in a similar manner.

7 Inclination properties and completion of the proof of Theorem 2

7.1 Inclination properties in chart K_1

Straightening the foliations We wish to track how $\mathcal{M}^{cu,+}$ passes through a neighborhood of the equilibrium p^+. We note that by the properties of the linearization about S_0^+, the manifolds $\mathcal{M}^{cu,+}$ and $W_1^{cu}(p^+)$ are both tangent to the collection of center-unstable eigenspaces of S_0^+. While they may not coincide due to the non-uniqueness of center manifolds, we find that they leave a neighborhood of p^+ exponentially close to each other.

As the vector-field in K_1 coordinates is C^s smooth for all $s \in \mathbb{N}$, the local center-stable and center-unstable manifolds possess the same regularity properties. Hence, classic results [7] give that there exists a C^{s-2} change of coordinates to $(w_s, w_u; w_{c,1}, w_{c,2})^T$, with $0 \in \mathbb{R}^4$ corresponding to p^+, which flattens the center manifold of p^+ along with its strong-stable and unstable foliations. For simplicity, we let $w_c = (w_{c,1}, w_{c,2})^T$. In such coordinates, the system takes the form

$$w_s' = \lambda_s w_s + g_s(w_s, w_u; w_c)w_s, \tag{7.1}$$

$$w_u' = \lambda_u w_u + g_u(w_s, w_u; w_c)w_u, \tag{7.2}$$

$$w_c' = h_c(w_c) + g_c(w_s, w_u; w_c), \tag{7.3}$$

where $\lambda_{u/s} = \pm\sqrt{2}$, $h_c : \mathbb{R}^2 \to \mathbb{R}^2$ gives the vector-field on the 2-D center manifold $\mathcal{M}^c$, and the nonlinearities satisfy

$$Dg_s(0,0;0) = 0 = Dg_u(0,0;0), \quad g_c(0, w_u; w_c) = g_c(w_s, 0; w_c) = 0. \tag{7.4}$$

We remark that the coordinates w_j used here are different than those used in the proof of Proposition 6.3. Hence the center stable and unstable manifolds are given as the invariant foliations of straight fibers

$$W_1^{cu}(p^+) = \bigcup_{|w_{c,0}| \leq \delta} \{w_c = w_{c,0}, \ w_s = 0, \ |w_u| \leq \delta\}, \qquad W_1^{cs}(p^+) = \bigcup_{|w_{c,0}| \leq \delta} \{w_c = w_{c,0}, \ w_u = 0, \ |w_s| \leq \delta\}.$$

We then define in and out sections, transverse to the flow of the system, which track how $\mathcal{M}^{cu,+}$ enters and leaves a neighborhood of p^+ locally near the sphere. We set,

$$\Sigma_1^{in} = \{(w_s, w_u, w_{c,1}, \rho) \ : \ |w_s| \leq \alpha, |w_u| \leq \beta, 0 \leq w_{c,1} \leq \delta\},$$

$$\Sigma_1^{out} = \{(w_s, w_u, \Delta, w_{c,2}) \ : \ |w_s| \leq \tilde{\alpha}, |w_u| \leq \tilde{\beta}, 0 \leq w_{c,2} \leq \tilde{\rho}\},$$

for some small positive constants $\alpha, \beta, \delta, \rho, \Delta, \tilde{\alpha}, \tilde{\beta}, \tilde{\rho}$.

Dynamics on the center-manifold We find that the vector-field h_c is unchanged in these straightened coordinates and the dynamics are governed by

$$w_{c,1}' = \frac{3w_{c,1}^2}{2}(1 - w_{c,2}^4), \tag{7.5}$$

$$w_{c,2}' = -\frac{w_{c,1}w_{c,2}}{2}(1 - w_{c,2}^4). \tag{7.6}$$

Using a change of coordinates $' = \dot{} \ (1 - r_1^4)^{-1}$, which preserves the direction of the flow for small enough values of r_1, one can obtain the partially decoupled system

$$\dot{w}_{c,1} = \frac{3w_{c,1}^2}{2}, \tag{7.7}$$

$$\dot{w}_{c,2} = -\frac{w_{c,1}w_{c,2}}{2}, \tag{7.8}$$

where $\cdot$ denotes differentiation with respect to the new variable $\tilde{\xi}_2$. This system can be explicitly solved to find that the solution with initial data $w_c(0) = (\epsilon_0, \rho)$, $0 < \epsilon_0 < \Delta$ lying in the section Σ_1^{in} has the form

$$(w_{c,1}, w_{c,2})(\tilde{\xi}_2) = \left(\frac{1}{\epsilon_0^{-1} - \frac{3}{2}\tilde{\xi}_2}, \ \rho(1 - \frac{3}{2}\epsilon_0\tilde{\xi}_2)^{1/3}\right),$$

and thus intersects the out section Σ_1^{out} where $w_{c,1}(\tilde{\xi}_{2,out}) = \Delta$ at the time $\tilde{\xi}_{2,out} = \frac{2}{3}(\epsilon_0^{-1} - \Delta^{-1})$. We also note that the corresponding $w_{c,2}$-component of the solution satisfies

$$w_{c,2}(\tilde{\xi}_{2,out}) = \rho\epsilon_0^{1/3}\Delta^{-1/3}. \tag{7.9}$$

Changing coordinates back to ξ_2-time, we obtain the transition time as

$$\xi_{2,out} = \frac{2}{3}(\epsilon_0^{-1} - \Delta^{-1})(1 - \mathcal{O}(\rho)).$$

Furthermore, we find that $w_{c,1}$ blows up in finite time at $\xi_2 = 2/(3\epsilon_0)$ while all initial conditions with $w_{c,1} > 0$ satisfy $\lim_{\xi_2 \to 2/(3\epsilon_0)} w_{c,2}(\xi_2) = 0$. Thus, we can define a transition map $\Pi_1 : \Sigma_1^{in} \to \Sigma_1^{out}$ for all points with $w_{c,1} \neq 0$, for constants α, β, ρ chosen suitably. (In particular, we require $w_{c,2}(\xi_{2,out}) \approx \rho(\epsilon_0\Delta^{-1})^{1/3} < \tilde{\rho}$, $\epsilon_0 < \Delta$, and β sufficiently small so that $|w_u(\xi_{2,out})| \leq \tilde{\beta}$.)

Next we wish to determine how $\mathcal{M}^{\text{cu},+}$ intersects Σ_1^{out}. Since, $\mathcal{M}^{\text{cu},+}$ is tangent to $\{w_s = 0\}$ along S_0^+, it can be written as a graph over the center-unstable space. In particular, the intersection with the in-section is given as

$$\Sigma_1^{in} \cap \mathcal{M}^{\text{cu},+} = \{(h_{\text{cu}}^{in}(w_u, w_{c,1}, \rho), w_u, w_{c,1}, \rho) : |w_u| \leq \beta, 0 \leq w_{c,1} \leq \delta\}, \tag{7.10}$$

for a C^r smooth function with $h_{\text{cu}}^{in}(0, 0, \rho) = 0$, $\partial_{w_u} h_{\text{cu}}^{in}(0, 0, \rho) = \partial_{w_{c,1}} h_{\text{cu}}^{in}(0, 0, \rho) = 0$.. The Sil'nikov coordinates then allow one to readily track such initial conditions forward to Σ_1^{out} using the straight foliation of the center manifold and an inclination result. In particular we find that Π_1 maps $\Sigma_1^{in} \cap \mathcal{M}^{\text{cu},+}$ onto a set which is exponentially close to $W_1^{\text{cu}}(p^+) = \{w_s = 0\}$.

Proposition 7.1. *For $0 < \delta < \Delta$ and $\Delta, \tilde{\beta}, \tilde{\rho} > 0$ sufficiently small, there exists a $C > 0$, such that the image of $\Sigma_1^{in} \cap \mathcal{M}^{\text{cu},+}$ under the transition map Π_1 in Σ_1^{out} can be written as a graph*

$$\Pi_1(\Sigma_1^{in} \cap \mathcal{M}^{\text{cu},+}) = \{(w_s^{out}, w_u^{out}, \Delta, w_{c,2}^{out}) : w_s^{out} = h_{\text{cu}}^{out}(w_u^{out}, w_{c,2}^{out}), \ 0 < w_{c,2}^{out} < \tilde{\rho}, \ |w_u^{out}| < \tilde{\beta}\}$$

with $h_{\text{cu}}^{out} : \mathbb{R}^2 \to \mathbb{R}$ C^r-smooth, satisfying

$$|h_{\text{cu}}(w_u^{out}, w_{c,2}^{out})| \leq Ce^{\frac{2\lambda_s}{3\Delta}((\rho/w_{c,2}^{out})^3 - 1)}, \quad 0 < w_{c,2}^{out} < \rho \tag{7.11}$$

uniformly for $|w_u^{out}| < \tilde{\beta}$.

Proof. We use a Sil'nikov boundary value formulation to write the w_s-coordinate of $\Pi_1(\Sigma_1^{in} \cap \mathcal{M}^{\text{cu},+})$ as a graph over the w_u^{out} and $w_{c,2}^{out}$ coordinates. In other words, we can write solutions with initial data in $\Sigma_1^{in} \cap \mathcal{M}^{\text{cu},+}$ solely in terms of the Σ_1^{out} data.

Using the straightened foliations of the strong stable and unstable dynamics, the results of [7] imply there exists a unique solution $(w_s, w_u, w_{c,1}, w_{c,2})(\xi; w_s^{in}, w_u^{out}, w_{c,1}^{in}, \rho)$ of the Sil'nikov boundary value problem with boundary data $w_c(0) = (w_{c,1}^{in}, \rho), w_s(0) = w_s^{in}, w_u(\xi_{2,out}) = w_u^{out}$ for $|w_{c,1}^{in}| \leq \delta$, $|w_s^{in}| \leq \alpha$, and $|w_u^{out}| \leq \tilde{\beta}$. Lemma 3.1 of [7] also gives that there exists exponential expansions of the solution components. In more detail, if $w_c^0(\xi)$ denotes the solution on the center manifold with initial condition $w_c^0(0) = w_c(0) = (w_{c,1}^{in}, \rho)$, then we have

$$w_c(\xi) = w_c^0(\xi) + R(\xi, \xi_{2,out}, w_s^{in}, w_u^{out}, w_{c,1}^{in}, \rho) \tag{7.12}$$

for some $\mathbb{R}^2$ valued C^{r-2}-function with $R(0, \xi_{2,out}, w_s^{in}, w_u^{out}, w_{c,1}^{in}, \rho) = 0$. This perturbation, as well as the hyperbolic parts of the solution satisfy the following estimates for some $C > 0$ independent of $\xi_{2,out}$ and the boundary data,

$$|w_s(\xi)| \leq Ce^{\lambda_s\xi}, \tag{7.13}$$
$$|w_u(\xi)| \leq Ce^{\lambda_u(\xi - \xi_{2,out})} \tag{7.14}$$
$$|R(\xi)| \leq Ce^{\lambda_s\xi + \lambda_u(\xi - \xi_{2,out})}. \tag{7.15}$$

With these general estimates, for each pair $(w_u^{out}, w_{c,1}^{in})$, we evaluate the w_u-component of the Sil'nikov solution at $\xi = 0$ and set $w_s^{in} = h_{\text{cu}}^{in}(w_u(0); w_{c,1}^{in}, \rho)$ where h_{cu}^{in} is the graph for the center-unstable manifold defined in (7.10) above. Furthermore, we also use

$$w_{c,2}^{out} = w_{c,2}(\xi_{2,out}) = \rho(w_{c,1}^{in}/\Delta)^{1/3} \cdot (1 + \mathcal{O}(\rho))$$

given above to write $w_{c,1}^{in}$ in terms of $w_{c,2}^{out}$, obtaining $w_{c,1}^{in} = \Delta(w_{c,2}^{out}/\rho)^3 \cdot (1 + \mathcal{O}(\rho))$. The graph h_{cu}^{out} is then given as the function

$$h_{\mathrm{cu}}^{out}(w_u^{out}, w_{c,2}^{out}) := w_s(\xi_{2,out}; w_s^{in}, w_u^{out}, w_{c,1}^{in}, \rho),$$

with the aforementioned substitutions for w_s^{in} and $w_{c,1}^{in}$. The estimates on h_{cu}^{out} then follow from using the substitutions and the exponential estimate on $w_s(\xi)$ above as well as the expansion,

$$\xi_{2,out} = \frac{2}{3}((w_{c,1}^{in})^{-1} - \Delta^{-1})(1 + \mathcal{O}(\rho)) = \frac{2}{3\Delta}\left((\rho/w_{c,2})^3 - 1\right)(1 + \mathcal{O}(\rho)).$$

$\square$

7.2 Inclination properties on chart K_3

One can also show that $W_3^{\mathrm{cs}}(p^0)$ is exponentially close to $\mathcal{M}^{\mathrm{cs},0}$ in a neighborhood of p_0 in the K_3 chart. The result follows in the same way as done in K_1 but one reverses time, flowing backwards from the "out" chart to the "in" chart. To this end one can once again change to coordinates $(w_s, w_u, w_{c,1}, w_{c,2})$ which straighten the strong fibers so that $W_3^{\mathrm{cs}}(p^0)$ is locally given by $\{w_u = 0\}$. Roughly $w_{c,1}$ corresponds to ϵ_3 and $w_{c,2}$ to r_3. We recall that the linearization at p^0 has hyperbolic eigenvalues $\tilde{\lambda}_u = 1, \tilde{\lambda}_s = -1$. One then defines in and out sections

$$\Sigma_3^{in} = \{(w_s, w_u, \Delta, w_{c,2}) : |w_s| \le \tilde{\alpha}, |w_u| \le \tilde{\beta}, 0 \le w_{c,2} < \rho\},$$
$$\Sigma_3^{out} = \{(w_s, w_u, w_{c,1}, \rho) : |w_s| \le \alpha, |w_u| \le \beta, 0 \le w_{c,2} < \delta\},$$

along with a transition map $\Pi_3 : \Sigma_3^{out} \to \Sigma_3^{in}$ formed by the time-reversed flow. Using the center manifold dynamics given by

$$w_{c,1}' = -\frac{3w_{c,1}^2}{2}(1 - w_{c,2}^4), \tag{7.16}$$

$$w_{c,2}' = \frac{w_{c,1}w_{c,2}}{2}(1 - w_{c,2}^4), \tag{7.17}$$

and a Sil'nikov boundary value problem, we then have the following inclination result.

Proposition 7.2. *For $0 < \delta < \Delta$ and $\Delta, \tilde{\beta}, \rho > 0$ sufficiently small, there exists a $C > 0$, such that the intersection of the image of $\Sigma_3^{out} \cap \mathcal{M}^{\mathrm{cs},0}$ under the transition map Π_3 in Σ_3^{in} can be written as a graph*

$$\Pi_3(\Sigma_3^{out} \cap \mathcal{M}^{\mathrm{cs},0}) = \{(w_s^{in}, w_u^{in}, \Delta, w_{c,2}^{in} : w_u^{in} = h_{\mathrm{cs}}^{in}(w_s^{in}, w_{c,2}^{in}), 0 < w_{c,2}^{in} < \rho, |w_s^{in}| < \tilde{\alpha}\},$$

with $h_{\mathrm{cs}}^{in} : \mathbb{R}^2 \to \mathbb{R}$ a C^r-smooth function satisfying

$$|h_{\mathrm{cs}}(w_s^{in}, w_{c,2}^{in})| \le Ce^{\frac{2\tilde{\lambda}_s}{3\Delta}\left((\rho/w_{c,2}^{in})^3 - 1\right)}, \quad 0 < w_{c,2}^{in} < \rho, \tag{7.18}$$

uniformly for $|w_s^{in}| < \tilde{\beta}$.

7.3 Tracking across the re-scaling chart and completion of proof of Theorem 2

To complete the proof, one translates the intersections $\Sigma_1^{out} \cap \mathcal{M}^{\mathrm{cu},+}$ and $\Sigma_3^{in} \cap \mathcal{M}^{\mathrm{cs},0}$ into the chart K_2 using κ_{12} and κ_{23}^{-1} respectively, and then flows them forward and backward respectively to construct an intersection in the section $\tilde{\Sigma}_2 = \{\mu_2 = 0\}$. In short, the existence of a 2-D intersection follows from the exponential closeness of $\Sigma_1^{out} \cap \mathcal{M}^{\mathrm{cu},+}$ to $\Sigma_1^{out} \cap W_1^{\mathrm{cu}}(p^+)$ and $\Sigma_3^{in} \cap \mathcal{M}^{\mathrm{cs},0}$ to $\Sigma_3^{in} \cap W_3^{\mathrm{cs}}(p^0)$, and the inclination properties about the transverse heteroclinic $u_2^* \in W_1^{\mathrm{cu}}(p^+) \cap W_3^{\mathrm{cs}}(p^0)$ in K_2.

For $(u_1, v_1, \epsilon_1, r_1) \in \Sigma_1^{out}$, recall we have $\epsilon_1 = \Delta$ and thus

$$(u_2, v_2, \mu_2, r_2) = \kappa_{12}(u_1, v_1, \Delta, r_1) = (\Delta^{-1/3}u_1, \Delta^{-2/3}v_1, \Delta^{-2/3}, \Delta^{1/3}r_1).$$

We then define the entry section in K_2 as $\Sigma_2^{in} = \kappa_{12}\Sigma_1^{out} = \{\mu_2 = \Delta^{-2/3}\}$ and set $\xi_{2,in} = -\Delta_1^{-2/3}$ so that $u_2^*(\xi_{2,in}) \in \Sigma_2^{in}$. For $(u_3, v_3, \epsilon_3, r_1) \in \Sigma_3^{in}$ we similarly have

$$(u_2, v_2, \mu_2, r_2) = \kappa_{23}^{-1}(u_3, v_3, \Delta, r_3) = (\Delta^{-1/3}u_3, \Delta^{-2/3}v_3, -\Delta^{-2/3}, \Delta^{1/3}r_3),$$

and thus define $\Sigma_2^{out} = \kappa_{23}^{-1}\Sigma_3^{in} = \{\mu_2 = -\Delta^{-2/3}\}$ and $\xi_{2,out} = \Delta_1^{-2/3}$ so that $u_2^*(\xi_{2,out}) \in \Sigma_2^{out}$.

Next, using the structure of κ_{12} and the result of Proposition 7.1, we have that $\mathcal{M}_{in} := \kappa_{12}(\Sigma_1^{out} \cap \mathcal{M}^{cu,+})$ is $\mathcal{O}(\Delta^{-2/3}\mathrm{e}^{-C/\Delta})$ away from $\kappa_{12}(\Sigma_1^{out} \cap W_1^{cu}(p^+))$ for some constant $C > 0$ for Δ sufficiently small and $r_1 < \rho/2$. Thus, we observe that $\mathcal{M}_{in}$ is a 2-D manifold in Σ_2^{in} which intersects the linear stable bundle $E^{s,-}(\xi_{2,in})$ transversely. Letting Φ_{ξ_2} denote the flow of (5.25) - (5.28) in K_2, the hyperbolic inclination properties about u_2^* then imply that $\Phi_{\xi_2}(\mathcal{M}_{in})$ exponentially converges onto $W_1^{cu}(p^+)$ as ξ_2 increases and can be written as a graph over the center-unstable bundle $E_2^{cu,-}(\xi_2)$. Using the monotonicity properties of the μ_2 flow for $0 \leq r_1 \ll 1$, the transition map $\Pi_{2,in} : \Sigma_2^{in} \to \tilde{\Sigma}_2$ defined by the flow Φ_{ξ_2} is well-defined, with time of flight $\xi_2 = -\Delta^{-2/3} + \mathcal{O}(r_2)$. Therefore we conclude that $\Pi_{2,in}\mathcal{M}_{in}$ can be written as a graph over $E^{cu,-}(0)$ and is exponentially close to $\tilde{\Sigma}_2 \cap W_1^{cu}(p^+)$ in a neighborhood of $u_2^*(0)$.

In a similar manner, Proposition 7.2, gives that $\mathcal{M}_{out} := \kappa_{23}^{-1}(\Sigma_3^{in} \cap \mathcal{M}^{cs,0})$ is $\mathcal{O}(\Delta^{-2/3}\mathrm{e}^{-C/\Delta})$ away from $\kappa_{23}^{-1}(\Sigma_3^{in} \cap W_3^{cs}(p_0))$ for $r_3 < \rho/2$. Defining $\Pi_{2,out} : \Sigma_2^{out} \to \tilde{\Sigma}_2$ by using the backwards flow $\Phi_{\xi_2}, \xi_2 < 0$, the inclination properties about u_2^* imply that $\Pi_{2,out}\mathcal{M}_{out}$ can be written as a graph over $E^{cs,+}(0)$ and is exponentially close to $\tilde{\Sigma}_2 \cap W_3^{cs}(p^0)$. Then using the transversality properties of the intersection $W_1^{cu}(p^+) \cap W_3^{cs}(p^0)$ we conclude the existence of the desired intersection, completing the existence result of Theorem 2.

Estimate (1.25) is obtained by putting the above results for charts K_1-K_3 together and translating back to the original coordinates. Here $\sqrt{2}w_{HM}$ is given by u_2^* in the K_2 coordinates. We see that the heteroclinic, formed by u_2^*, obtained in the singular limit of the above geometric desingularization analysis is the leading-order approximation of the desired front solution in the region $|\mu| \lesssim \rho\epsilon^{2/3}$, where $\rho > 0$ is a small, ϵ independent constant. Moreover, given that $\mu \sim -\epsilon\xi$ in a neighborhood of the origin, the leading order asymptotics hold for $|\xi| \leq \rho\epsilon^{-1/3}$. Unwinding the scalings from the blow-up coordinates, the desired heteroclinic front solution asymptotically satisfies

$$|u^*(\xi) - \epsilon^{1/3}u_2^*(\epsilon^{1/3}\xi)| \leq \rho\epsilon^{2/3}, \qquad |\xi| \leq \rho\epsilon^{-1/3}. \tag{7.19}$$

8   Discussion and future directions

To conclude, we discuss several immediate consequences of our results and highlight several avenues for future research. We expect our $c > 0$ results and the phenomenological mechanisms studied in this work to govern front dynamics for any scalar reaction-diffusion equation

$$u_t = u_{xx} + f(x - ct, u), \quad u(x,t) \in \mathbb{R}, \tag{8.1}$$

where f is smooth with slowly varying heterogeneity which moderates the stability of a homogeneous equilibrium state and undergoes a bifurcation to a stable equilibrium state as ξ moves from $+\infty$ to $-\infty$. For example, we expect a result similar to Theorem 1 to hold for (8.1) for a slowly-varying Fisher-KPP type nonlinearity $f(\xi, u) = \mu(\xi)u - u^2$ with μ defined as above. Furthermore, we expect the underlying mechanisms studied here to govern the formation of front solutions in slowly-varying super-critical pattern-forming equations, such as the real and complex Ginzburg-Landau equations, the Swift-Hohenberg equation, and many relevant reaction-diffusion equations.

This work can be viewed as a new contribution to the nascent body of research studying dynamic bifurcation in spatially extended systems. It points to a new set of problems which are of interest both for applications and for mathematics. It also provides a novel application-motivated example of how techniques from geometric singular perturbation theory can be used to uncover and precisely characterize front dynamics in a slowly-varying environment. From a technical perspective, it also provides a testbed to apply dynamic bifurcation techniques in a higher-order system with multiple additional hyperbolic directions as well as a control parameter (in our case c) which governs the specific type of dynamic bifurcation.

8.1   Stability

It is not difficult to see that the solutions constructed in Theorem 1 and Theorem 2 are asymptotically stable, that is, they attract all nearby initial conditions exponentially in the equation (1.1), posed in the co-moving frame $\zeta = -(x - ct)$,

$$u_t = u_{\zeta\zeta} - cu_\zeta + \mu u - u^3 \tag{8.2}$$

Given standard results on asymptotic stability in semilinear PDE (see [19, Ch. 5] or [24]), it is sufficient to show that the spectrum of the linearization at such a solution has strictly negative real part. Note that there

is no spatial translation eigenvalue due to the heterogeneity. We write therefore u^* for the first component of Γ_ϵ, suppressing the dependence on ϵ and c, and recall that $u^*_\zeta > 0$ and $\mu_\zeta > 0$. We then need to consider the spectrum of the linearization

$$\mathcal{L}_0 u := u_{\zeta\zeta} - cu_\zeta + (\mu - 3(u^*)^2)u, \tag{8.3}$$

considered as a closed and densely defined operator on, say $BC^0(\mathbb{R})$. This operator is conjugate to a formally self-adjoint operator

$$\mathcal{L}_c u := (e^{-c\zeta/2}\mathcal{L}_0 e^{c\zeta/2})u = u_{\zeta\zeta} + (\mu - \frac{c^2}{4} - 3(u^*)^2)u, \tag{8.4}$$

Indeed, $\mathcal{L}_c$ is clearly self-adjoint on $L^2(\mathbb{R})$. A quick calculation shows that the essential spectra of $\mathcal{L}_0$ and $\mathcal{L}_c$ have strictly negative real part. Moreover, inspecting the decay of eigenfunctions, that is, to solutions of $\mathcal{L}_c u = \lambda u$ with $\text{Re}\lambda \geq 0$, one quickly sees that the point spectra of $\mathcal{L}_0$ and $\mathcal{L}_c$ coincide. Similarly, point and essential spectra do not depend on the choice BC^0 versus L^2, so that we restrict ourselves to excluding eigenvalues $\lambda \geq 0$ to $\mathcal{L}_c$ in L^2.

To exclude such eigenvalues, we proceed as in Proposition 6.2 above. Assume that there is a maximal eigenvalue $\lambda_0 \geq 0$ with eigenfunction $u_0(\zeta)$, which then has a sign and we assume $u_0(\zeta) > 0$. Next, recall that $u^*_{\zeta\zeta} - cu^*_\zeta + \mu u^* - (u^*)^3 = 0$, so that, by differentiating with respect to ζ, we find

$$\mathcal{L}_0 u^*_\zeta + \mu_\zeta u^* = 0, \tag{8.5}$$

or

$$\mathcal{L}_c \left(e^{-c\zeta/2}u^*_\zeta\right) + \left(e^{-c\zeta/2}\mu_\zeta\right)u^* = 0. \tag{8.6}$$

One quickly verifies that $\left(e^{-c\zeta/2}u^*_\zeta\right)$ is exponentially localized, as is $\left(e^{-c\zeta/2}\mu_\zeta\right)u^*$, and we shall exploit this property by testing the eigenvalue against these functions. We find from $\mathcal{L}_c u_0 = \lambda u_0$ after integrating against $e^{-c/2}u^*_\zeta$, that, using first that $u^*_\zeta, u_0 > 0$, $\lambda_0 \geq 0$, self-adjointness of $\mathcal{L}_c$, and (8.6),

$$\left\langle e^{-c\zeta/2}u^*_\zeta, \mathcal{L}_c u_0 \right\rangle_{L^2} = \lambda_0 \left\langle e^{-c\zeta}u^*_\zeta, u_0 \right\rangle_{L^2} \geq 0,$$
$$\left\langle \mathcal{L}_c(e^{-c\zeta/2}u^*_\zeta), u_0 \right\rangle_{L^2} \geq 0,$$
$$\left\langle -e^{-c\zeta/2}\mu_\zeta u^*, u_0 \right\rangle_{L^2} \geq 0,$$

a contradiction to $\mu_\zeta, u^*, u_0 > 0$.

Non-monotone fronts, discussed next, are likely unstable with increasing Morse index. Using Maslov index arguments, for example, one would seek to establish the additional unstable eigenvalues for each node created in the solution.

Remark 8.1. *For slowly-ramped fronts in systems without a comparison principle and the monotonicity properties exploited above, the techniques of [14] should be of use in locating spectrum and proving stability. In more detail, the front u^* is exponentially close to the trivial state $u = 0$ in the $\mathcal{O}(\epsilon^{2/3})$-wide interval $\mu \in (\mu_{\text{fr}}, \mu_c)$. Here, the trivial state is absolutely unstable. Since this region is $\mathcal{O}(\epsilon^{-1/3})$-wide in the spatial variable ξ, one expects all but finitely many of the point spectrum of $\mathcal{L}$ to lie close to the absolute spectrum of the trivial state. Following the aforementioned work, one would projectivize the eigenvalue problem $\mathcal{L}v = \lambda u$ and track the slow winding of the unstable subspace as ξ passes from ξ_{fr} to ξ_c. Since the winding frequency slows to zero as ξ increases and $\mu \to \mu_c^-$, one does not expect intersections to exist for $\lambda \geq 0$, and thus no unstable eigenvalues.*

8.2 Fronts with non-monotonic tails

As briefly mentioned in the introduction, our approach for dynamic quenching can readily be extended to prove the existence of fronts with oscillatory tails as well as for fronts with $\lim_{\zeta\to+\infty} u(\zeta) = -1$. Such fronts arise from the slow attracting manifold S^a_ϵ on the plane U_0, and its corresponding strong unstable foliation, winding all the way around the cylinder before intersecting the stable manifold. After S^a_ϵ passes around the fold point, the z-dynamics in (2.6) cause the manifold to blow-up to negative infinity in finite time. This corresponds to the trajectory moving to another chart of the cylinder. Dynamics on this chart can be coordinatized with a blow-up in the v-direction, $w = v/u$, where $w = 0$ roughly corresponds to $z = \infty$. On the invariant cylinder the dynamics are governed by the equation

$$w_\zeta = 1 - cw + (\theta + c^2/4)w^2$$

and thus consist of constant drift at leading order for $w \sim 0$. After tracking the slow manifold through this chart one would then study the dynamics in the $-u$ blow-up with the coordinate $\hat{z} = -v/u$ and find intersections of the unstable manifold with the stable manifold of the $u = -1$ equilibrium. Further tracking it around the cylinder back to the original chart one could then find another intersection with the original stable manifold. We once again remark that one could use a polar coordinate blowup of the dynamics near $(u, v) = (0, 0)$ without the use of charts. See Figure 8.1 for a schematic depiction. These dynamics are similar those found in the work [2] which finds Airy points along the repelling slow manifold of the Fitzhugh-Nagumo system, where the local linear stability type of the point in the fast subsystem changes from being an unstable node to an unstable spiral. As we expect the fronts with non-trivial winding around the cylinder to be unstable, we do not rigorously pursue their existence here.

Interestingly, non-monotonicity can also result from a small bias in the cubic, leading to a Painlevé II equation with an asymmetric cubic $\eta w + 2w^3 + k$ for some $k > 0$. We expect a variety of interesting applications and more complex results relating to the competition between pulled and pushed fronts, and refer to [42] for a discussion of applications and analysis of relevant, non-monotone, special solutions in the stationary case $c = 0$.
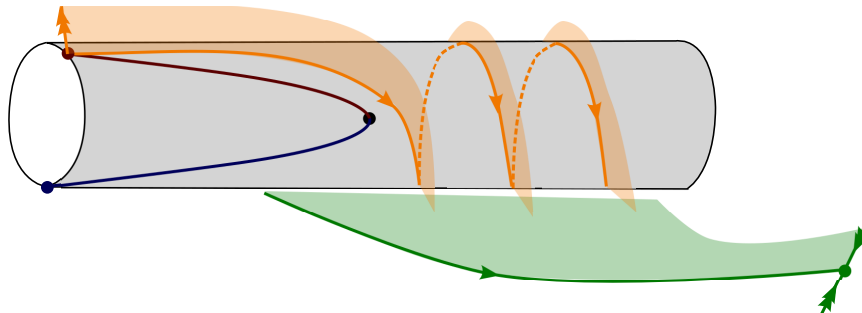

Figure 8.1: Schematic depiction of dynamics near the polar coordinate blow-up of the line $(0, 0, \mu)$ into the cylinder $\{r = 0\}$ (grey). Colors correspond to objects depicted in previous figures. Winding of the unstable manifold $W^u(0, 0, -1)$, which in the blow-up coordinates consists of the attractive slow manifold S^a_ϵ in the cylinder (orange trajectory) and its strong unstable foliation (orange sheet), allows for additional intersections between the stable manifold $W^s(1, 0, 1)$ (green). Red and blue curves denote the $\epsilon = 0$ curves of equilibria. Furthermore, this winding allows for connections with the stable manifold $W^s(-1, 0, 1)$ of the other equilibrium, $u \equiv 1$, at $\mu = 1$ (not depicted).

8.3 Fronts for asymptotically small speeds $0 < c \ll 1$

We now discuss front solution behavior and asymptotics in the limit where the quenching speed c is asymptotically small. First of all, numerical results in Figure 8.2 of the difference $\mu_{\text{fr}} - \mu_c$, show that as c decreases, the ϵ interval on which the $\epsilon^{2/3}$-delay is valid shrinks. In other words, we observe that as c decreases, the value of ϵ_0 given in Theorem 1 goes to zero. Indeed for sufficiently small c, the front interface lies ahead of μ_c so that $\mu_{\text{fr}} - \mu_c < 0$, at least for the numerical range of values ϵ used in computation. Thus the front tail bleeds into the region where $\mu \leq 0$. From a PDE perspective this advance of the front tail could be viewed as being caused by the comparatively large role diffusion plays when the quench is slow moving. Also, we find below that for such small speeds, the front profile resembles the unique connecting solution of Painlevé's second equation observed in the $c = 0$ case discussed in Section 5 above.

To understand this behavior one could alternatively seek to understand the limit $c \to 0^+$ for ϵ fixed small. Such numerics are also depicted in the right plot of Figure 8.2. We find, as c decreases the front follows $\sqrt{\mu}$ for a larger range of ξ but decays more slowly as ξ increases past 0. Furthermore, we can also track the change in front behavior by tracking the value $u(\xi_c)$, where ξ_c is such that $\mu(\xi_c) = \mu_c$. This indicates the size of the front at the leading order take off point. Since there is an additional delay in the front interface for ϵ sufficiently small, we expect these values to remain exponentially small. In Figure 8.3, we indeed find that the interval of ϵ values where u is exponentially small decreases as c decreases. In the limit $c = 0$, there is no such interval and a linear fit of the log-log data here indicates that $u(\xi_c = 0)$ scales like $\epsilon^{1/3}$.

Further evidence that there is a transition at $c \sim \epsilon^{1/3}$ in the dynamics of the fronts comes from some preliminary analysis. On the one hand, for asymptotically small values of c which satisfy $c \ll \epsilon^{1/3}$, it turns out that the system is again a perturbation of the Painlevé II equation, as is the case for $c = 0$. Indeed, for $c > 0$, one starts with system (5.6)-(5.9) and adds the term $-cv$ to the second component. For asymptotically small

values $c = \epsilon^\sigma \tilde{c}$ where $\tilde{c} = \mathcal{O}(1)$ with respect to ϵ, one may use the same dynamically rescaled coordinates (5.10) and the same method of geometric desingularization as used above. In particular, in the rescaling chart K_2, one finds the same system (5.25)-(5.28), as in the analysis of the case $c = 0$, but now with the term $-r_2^{3\sigma-1}\tilde{c}v_2$ included in the second component, (5.26). This term is a small perturbation term for $0 < r_2 \ll 1$ as long as $\sigma > 1/3$. Hence, for $c \ll \epsilon^{1/3}$, the structure of the full system is also that of a small perturbation of the Painlevé II equation, as above in the analysis for $c = 0$.

On the other hand, for asymptotically small values of c which satisfy $c \gg \epsilon^{1/3}$, preliminary analysis suggests that one can extend the method of proof of Theorem 1 down to $c \gg \epsilon^{1/3}$. For asymptotically small values of c, the boundary of U_0^r at $\{z = -c/2\}$ gets close to the axis, and with $c \gg \epsilon^{1/3}$, the method of Sections 2-4 can still be used to show that the invariant manifolds intersect transversely. Moreover, the terms in the asymptotic expansion (1.14) stay well ordered for $c \gg \epsilon^{1/3}$.
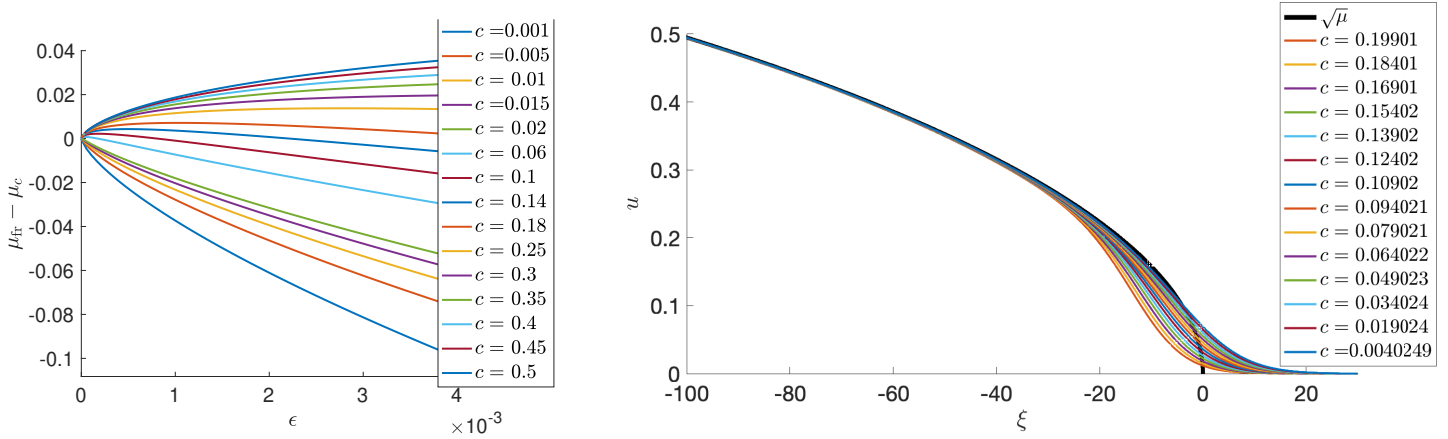

Figure 8.2: Left: plots of the numerically measured difference $\mu_{\mathrm{fr}} - \mu_c$ against ϵ, for a range of c values (given in legend), curves increase as c increases; Right: Plots of the front profile near $\mu = 0$ for a range of c-values (in legend), curves decrease as c increases with $\epsilon = 0.0025$ fixed.
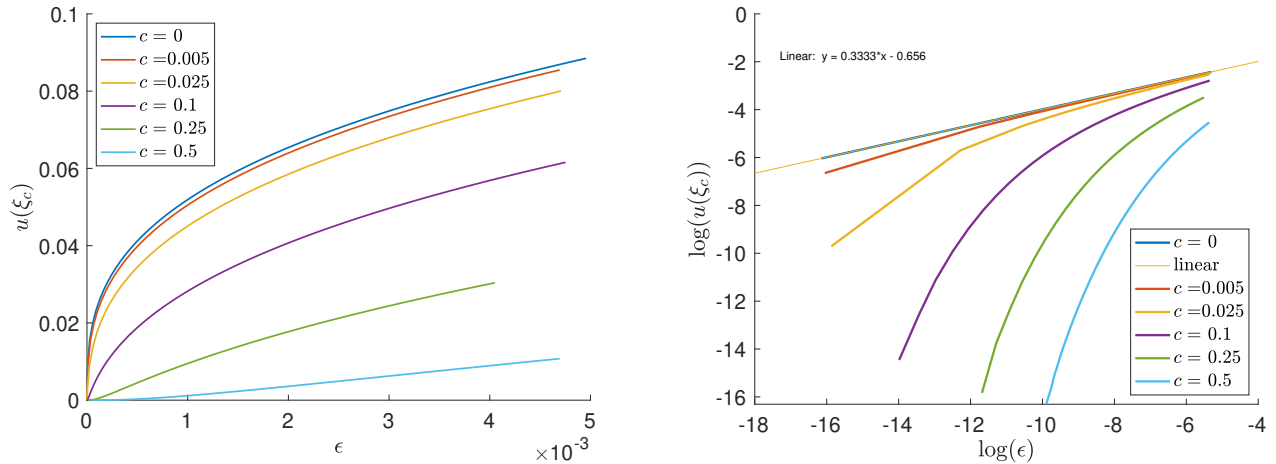

Figure 8.3: Left: plot of the values $u(\xi_c)$ against ϵ for a range of speeds c. Note the curves from convex to concave as c decreases; Right: Log-log plot of $u(\xi_c)$ against ϵ, showing that the front height becomes exponentially small in ϵ for moderate speeds c. Also included is a linear fit of the $c = 0$ curve (light yellow, with fit equation printed), indicating that $u(\xi_c)$ scales like $\epsilon^{1/3}$ in this case.

8.4 $c > 2$ and spatially homogeneous slow quenches

As mentioned in the introduction, we expect no traveling wave solutions to exist for quenching speeds $c > 2$. In the full dynamics of the PDE (1.1), since μ approaches 1 as $t \to +\infty$ for all points $x \in \mathbb{R}$, we expect compactly supported perturbations to spread with asymptotic speed 2. To characterize this regime, we introduce an altered

parameterization of the quench

$$u_t = u_{xx} + \mu(\alpha x - t)u - u^3, \tag{8.7}$$

$$\mu(\eta) = -\tanh(\epsilon\eta), \quad \mu(0) = 0. \tag{8.8}$$

with a new traveling wave variable $\eta = \alpha x - t$. Here the new parameter $\alpha \in \mathbb{R}$ gives the speed of the moving quench as $1/\alpha$, and thus the range $\alpha > 1/2$ corresponds to the case $c \in (0, 2)$ studied above, while the range $\alpha \in (0, 1/2)$ corresponds to $c > 2$, and $\alpha = 0$ to a spatially homogeneous quench which uniformly renders the trivial state unstable. In the latter two cases, one immediate question of interest is how the front interface moves and how its speed asymptotically approaches 2. In the $\alpha = 0$ case, where μ slowly varies from -1 to 1 as time evolves from $t = -\infty$ to $t = +\infty$, uniformly in x, a leading-order heuristic prediction can be obtained using a simple characteristic argument. The uniform growth of μ causes perturbations of the trivial state to accelerate their growth as $t > 0$ increases. Since the growth is slow, one "freezes coefficients" so that the predicted instantaneous invasion speed at each fixed $t > 0$ is given as $s(t) = 2\sqrt{\mu(t)}$. Hence, given a localized perturbation lying near the origin with support contained in $[-x_0, x_0]$ for some x_0, one predicts the front location $x_{\mathrm{fr}}(t)$ to satisfy the characteristic equation

$$\frac{dx_{\mathrm{fr}}}{dt} = s(t), \qquad x_{\mathrm{fr}}(0) = x_0,$$

and hence is given as

$$x_{\mathrm{fr,pred}}(t) = x_0 + \int_0^t 2\sqrt{\mu(\sigma)}d\sigma. \tag{8.9}$$

For $\mu(\eta) = -\tanh(\epsilon\eta)$, or alternatively for a purely linear ramp $\mu(\eta) = \epsilon\eta$, it is possible to obtain $x_{\mathrm{fr,pred}}(t)$ in closed form. See Figure 8.4 for a comparison of the numerically measured front location $x_{\mathrm{fr,num}}$ and this prediction. We find, after an initial transient where the front establishes itself, the front location moves slightly faster than the prediction.

A simple heuristic argument supporting this finding goes as follows. The linear spreading in the stationary frame of a perturbation of the trivial state with exponential decay $\sim \mathrm{e}^{\nu x}$ is determined by a quantity known as the *envelope velocity*, defined as $s_{\mathrm{env}}(\nu) = -\mathrm{Re}\lambda(\nu)/\mathrm{Re}\,\nu$, where $\lambda(\nu)$ is a root of the linear dispersion relation (1.6) with $c = 0$. For a given μ and $\nu \in \mathbb{R}$, we find $s_{\mathrm{env}}(\nu) = -\frac{\nu^2 + \mu}{\nu}$. The linear spreading speed discussed is related to the envelope speed through $s_{\mathrm{lin}} = \min_{\nu \in \mathbb{R}} s_{\mathrm{env}}(\nu) = 2\sqrt{\mu}$. In the stationary frame, the $\nu < 0$ (corresponding to rightward spreading waves) which minimizes the envelope velocity is given as $\nu = -\sqrt{\mu}$. Now let us return back to the slowly-varying quench $\mu = \mu(t)$. At a given fixed time $t_1 > 0$, the above prediction for the invasion speed $s(t_1) = 2\sqrt{\mu(t_1)}$ would have a front with spatial decay $\nu(t_1) = -\sqrt{\mu(t_1)}$. Now for a time t_2 just after t_1, where μ has increased further, the envelope speed of this tail $s_{\mathrm{env}}(\nu(t_1))$ is greater than the predicted instantaneous speed for $\mu(t_2)$. Hence we expect the front to accelerate faster than predicted in calculation (8.9). We anticipate that one can obtain a more refined prediction, as well as rigorous existence and asymptotics, by explicitly solving the linearized equation $v_t = v_{xx} + \mu(t)v$ to understand spreading asymptotics of exponential tails and then construct fronts using comparison principle methods.

A   The potential is sign definite.

In this appendix, we prove that the potential obtained from linearizing the Painlevé II equation about the Hastings-McLeod solution is sign definite. This result (see Lemma A.2 below) is not only of use as a direct way to show in Proposition 6.2 that the ground state is sign definite, as remarked above, but it is also of independent interest for the Painlevé II equation. Given the independent interest, we prove the result using the standard form (1.17) of the equation.

Lemma A.1. *(Hastings [17]) For the Hastings-McLeod solution, $w(\eta)$ of the Painlevé II equation $w'' = \eta w + 2w^3$, one has the following lower bound: $w(\eta = 0) \geq \mathrm{Ai}(0) = \frac{1}{3^{2/3}\Gamma(\frac{2}{3})}$.*
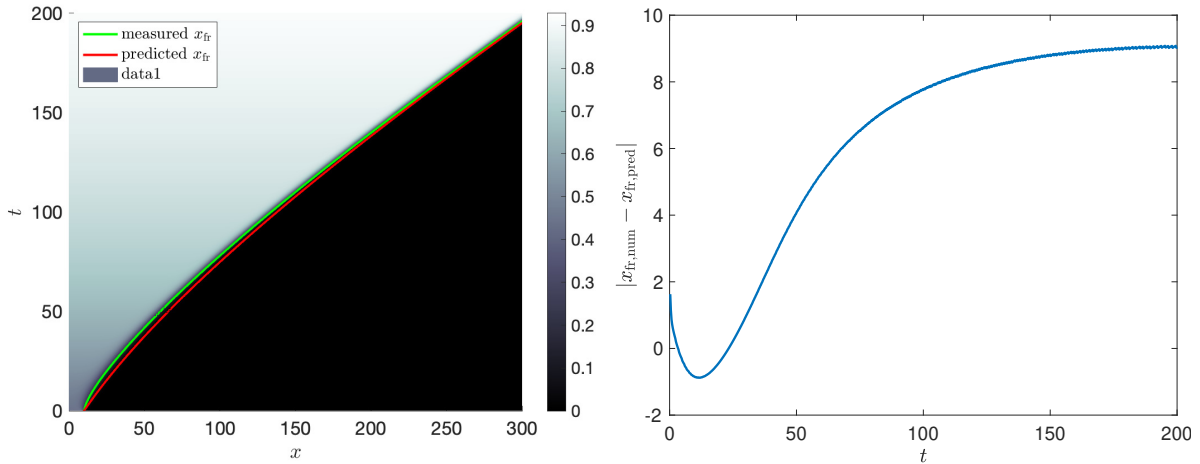
Figure 8.4: Direct numerical simulation of (8.7) with $\epsilon = 0.005, \alpha = 0$; left: Spacetime diagram of the solution with measured front location $x_{\text{fr,num}}$ (green) where $u(x,t) = 0.2$ and prediction of $x_{\text{fr,pred}}$ from (8.9); right: depiction of the difference between the measured and predicted front location.

Proof. This lemma and its proof are due to Professor Stuart Hastings [17]. By Theorem 2 of [18], it is known that $\lim_{\eta \to \infty} \frac{w(\eta)}{\text{Ai}(\eta)} = 1$. So, suppose that $w(0) < \text{Ai}(0)$. Then, there is an $\eta_R > 0$ at which $\left(\frac{w}{\text{Ai}}\right)' > 0$. Hence, at η_R, one has $w'\text{Ai} - \text{Ai}'w > 0$. Next, observe that $\left(w'\text{Ai} - \text{Ai}'w\right)'(\eta) = 2(w(\eta))^3\text{Ai}(\eta) > 0$ for all $\eta \geq 0$, which implies that

$$\left(\frac{w}{\text{Ai}}\right)' = \frac{w'\text{Ai} - \text{Ai}'w}{\text{Ai}^2} \to \infty, \quad \text{as} \ \ \eta \to \infty.$$

This contradicts the asymptotics of $w(\eta)$. Hence, the supposition that $w(0) < \text{Ai}(0)$ is incorrect, and the lemma is proven. $\qquad\square$

Lemma A.1 is used as a key step in establishing the following result about the potential $\mathcal{V}(\eta) = \eta + 6(w(\eta))^2$, obtained by linearizing the right hand side of the Painlevé II equation about the Hastings-McLeod solution.

Lemma A.2. *The potential* $\mathcal{V}(\eta) = \eta + 6(w(\eta))^2$ *evaluated along the Hastings-McLeod solution* $w(\eta)$ *of the second Painlevé equation* $w'' = \eta w + 2w^3$ *is strictly positive for all* $\eta \in \mathbb{R}$.

Proof. First, for all $\eta \geq 0$, one sees directly that $\mathcal{V}(\eta) > 0$, since $w(\eta) > 0$ for all η by Theorem 1 of [18]. Also, $\mathcal{V}(\eta) > 0$ for $\eta_0 \leq \eta < 0$, where $\eta_0 < 0$ is the unique point at which $w''(\eta) = 0$ (recall Theorem 1 of [18]), since $\left(\eta + 2(w(\eta))^2\right)w(\eta) = w''(\eta) > 0$ for all $\eta > \eta_0$ and $w > 0$ for all η.

The difficult part of the proof is to show that $\mathcal{V}(\eta) > 0$ also for all $\eta < \eta_0$. This may be accomplished as follows. The potential $\mathcal{V}(\eta) \to \infty$ as $\eta \to -\infty$. Hence, there is some $\eta_L < 0$ sufficiently negative such that $\mathcal{V}(\eta) > 0$ on $(-\infty, \eta_L]$. Now, on the interval (η_L, η_0), we use the coordinate change $w(\eta) = \sqrt{-\eta/2}\, z(\eta)$. Here, $z(\eta)$ satisfies $\frac{d^2 z}{d\eta^2} + \frac{1}{\eta}\frac{dz}{d\eta} = \frac{z}{4\eta^2} + \eta z(1 - z^2)$, which is equation (2.4) with $\alpha = 0$ in [18]. It suffices to show that $\mathcal{V}$, which is now $\mathcal{V}(\eta) = (-\eta)(3z^2 - 1)$, is strictly positive at any local minimum of $\mathcal{V}$ on (η_L, η_0). At a local minimum η_m of $\mathcal{V}$, $\frac{dz}{d\eta}(\eta_m) = \frac{3(z(\eta_m))^2 - 1}{-6\eta_m z(\eta_m)}$. Substituting this into the condition that $\frac{d^2\mathcal{V}}{d\eta^2} > 0$ at a local minimum, one finds that $(z(\eta_m))^2 - 1 > \frac{1}{36(z(\eta_m))^4(\eta_m)^3}$ at any local minimum of $\mathcal{V}$ on this interval. Hence, at a local minimum, the key term in the potential satisfies

$$3(z(\eta_m))^2 - 1 > 2(z(\eta_m))^2 + \frac{1}{36(z(\eta_m))^4(\eta_m)^3}.$$

Now, the term in the right member is strictly positive as long as $w(\eta_m) = \sqrt{-\eta_m/2}\, z(\eta_m) > (576)^{-1/6} = 0.34668\ldots$, as may be seen by a straightforward calculation. Moreover, $w(\eta_m) > w(0)$, since $\frac{dw}{d\eta}(\eta) < 0$ for all η by Theorem 1 of [18], and $w(0) > \text{Ai}(0) = \frac{1}{3^{2/3}\Gamma\left(\frac{2}{3}\right)} = 0.355028\ldots$, by Lemma 1. Therefore, $3(z(\eta_m))^2 - 1 > 0$ at any local minimum on (η_L, η_0), and hence $\mathcal{V}(\eta) > 0$ for all $\eta \in (\eta_L, \eta_0)$. This completes the proof of the lemma. $\qquad\square$

The proof of Lemma A.2 involves analysis of local minima of $\mathcal{V}$ and relies on Lemma A.1. An alternative proof of the positivity of the potential $\mathcal{V}$ evaluated along the Hastings-McLeod solution w may be obtained using the method of proof by contradiction, as follows:

Lemma A.3. *(Hastings [17]) The Hastings-McLeod solution $w(\eta)$ of the second Painlevé equation satisfies $w(\eta) > \sqrt{-\eta/6}$ for $\eta \in (-\infty, 0]$.*

Proof. For each $\alpha \geq 6$, define $f_\alpha(\eta) = \sqrt{-\eta/\alpha}$ on $(-\infty, 0]$. Since $w(\eta) \sim \sqrt{-\eta/2}$ as $\eta \to -\infty$, there exists an $\eta_L < 0$ such that $f_6(\eta) < w(\eta)$ for $\eta \leq \eta_L$. Moreover, since $f_\alpha(\eta) < f_6(\eta)$ for $\alpha > 6$ on $(-\infty, 0)$, $f_\alpha(\eta) < w(\eta)$ on $(-\infty, \eta_L]$ for all $\alpha > 6$, as well.

Next, since $f_\alpha \to 0$ as $\alpha \to \infty$ uniformly on $[\eta_L, \infty)$, there is an $\alpha_L > 0$ such that $f_\alpha(\eta) < w(\eta)$ on $(-\infty, 0]$ for all $\alpha \geq \alpha_L$. Hence, if there is a point η at which $f_\alpha(\eta) = w(\eta)$ for some $\alpha \geq 6$, then that point η must lie in $[\eta_L, 0]$. Also, if this is true for some $\alpha \geq 6$, then there must exist a greatest such value, call it α^*. Moreover, any point of intersection of f_{α^*} with w must be a point of tangency, with $f_{\alpha^*}(\eta) \leq w(\eta)$ on $(-\infty, 0]$, otherwise by continuity α^* would not be the greatest value.

Now, suppose that η^* is such a point of tangency between f_{α^*} and w. At η^*, one has $f_{\alpha^*} = w > 0$, $f'_{\alpha^*} = w' < 0$, and $f''_{\alpha^*} \leq w''$ (where the sign of w'' is unknown). Also, one has $w'' = \eta^* w + 2w^3 = \eta^* f_{\alpha^*} + 2f_{\alpha^*}^3$. Then, calculating f''_{α^*}, one obtains $\frac{-1}{4\alpha^{*2} f_{\alpha^*}^3} \leq \eta^* f_{\alpha^*} + 2f_{\alpha^*}^3$. In turn, this implies that $\frac{-1}{4\alpha^{*2}} \leq \eta^* f_{\alpha^*}^4 + 2f_{\alpha^*}^6 = \frac{\eta^3}{\alpha^{*2}}\left(1 - \frac{2}{\alpha^*}\right) \leq \frac{\eta^3}{\alpha^{*2}}\left(1 - \frac{2}{6}\right) < 0$. Hence, $\eta^{*3} \geq -\frac{3}{8}$, and one may bound η^* from below as $\eta^* \geq -0.73$. Thus, for any such $\alpha^* \geq 6$, one finds that $w(\eta^*) = f_{\alpha^*}(\eta^*) \leq 0.349$. However, this is a contradiction, since $w(\eta^*) > w(0) \geq \frac{1}{3^{2/3}\Gamma(2/3)} \geq 0.355$, by Lemma A.1. Therefore, there cannot be any such $\alpha^* \geq 6$, and we have $f_6(\eta) < w(\eta)$ for all $\eta \in (-\infty, 0]$. This completes the proof of the lemma. $\square$

References

[1] J. Baik, R. Buckingham, and J. DiFranco. Asymptotics of Tracy-Widom distributions and the total integral of a Painlevé II function. *Communications in Mathematical Physics*, 280:463–497, 06 2008.

[2] P. Carter and B. Sandstede. Unpeeling a homoclinic banana in the Fitzhugh–Nagumo system. *SIAM Journal on Applied Dynamical Systems*, 17(1):236–349, 2018.

[3] P. A. Clarkson. Painlevé equations—nonlinear special functions. *Journal of computational and applied mathematics*, 153(1-2):127–140, 2003.

[4] N. J. Cleri and G. V. Dunne. Resurgent trans-series for generalized Hastings–McLeod solutions. *Journal of Physics A: Mathematical and Theoretical*, 53(35):355203, aug 2020.

[5] A. Couairon and J.-M. Chomaz. Fully nonlinear global modes in slowly varying flows. *Physics of Fluids*, 11(12):3688–3703, 1999.

[6] P. A. Deift and X. Zhou. Asymptotics for the Painlevé II equation. *Communications on Pure and Applied Mathematics*, 48(3):277–337, 1995.

[7] B. Deng. Homoclinic bifurcations with nonhyperbolic equilibria. *SIAM Journal on Mathematical Analysis*, 21(3):693–720, 1990.

[8] *NIST Digital Library of Mathematical Functions*. http://dlmf.nist.gov/, Release 1.1.6 of 2022-06-30. F. W. J. Olver, A. B. Olde Daalhuis, D. W. Lozier, B. I. Schneider, R. F. Boisvert, C. W. Clark, B. R. Miller, B. V. Saunders, H. S. Cohl, and M. A. McClain, eds.

[9] E. J. Doedel, A. R. Champneys, F. Dercole, T. F. Fairgrieve, Y. A. Kuznetsov, B. Oldeman, R. Paffenroth, B. Sandstede, X. Wang, and C. Zhang. Auto-07p: Continuation and bifurcation software for ordinary differential equations. 2007.

[10] T. A. Driscoll, N. Hale, and L. N. Trefethen. *Chebfun Guide*. Pafnuty Publications, 2014.

[11] J. Feng, W.-H. Hsu, D. Patterson, C.-S. Tseng, H.-W. Hsing, Z.-H. Zhuang, Y.-T. Huang, A. Faedo, J. L. Rubenstein, J. Touboul, and S.-J. Chou. COUP-TFI specifies the medial entorhinal cortex identity and induces differential cell adhesion to determine the integrity of its boundary with neocortex. *Science Advances*, 7(27):eabf6808, 2021.

[12] N. Fenichel. Geometric singular perturbation theory for ordinary differential equations. *Journal of Differential Equations*, 31(1):53–98, 1979.

[13] R. Goh. Quenched stripes: Wavenumber selection and dynamics. *SIAM DSWeb*, 2021.

[14] R. Goh and B. de Rijk. Spectral stability of pattern-forming fronts in the complex Ginzburg–Landau equation with a quenching mechanism. *Nonlinearity*, 35(1):170, 2021.

[15] R. Goh and A. Scheel. Triggered fronts in the complex Ginzburg Landau equation. *Journal of Nonlinear Science*, 24(1):117–144, 2014.

[16] R. Haberman. Slowly varying jump and transition phenomena associated with algebraic bifurcation problems. *SIAM Journal on Applied Mathematics*, 37(1):69–106, 1979.

[17] S. P. Hastings. Private communication. 2022.

[18] S. P. Hastings and J. B. McLeod. A boundary value problem associated with the second Painlevé transcendent and the Korteweg-de Vries equation. *Archive for Rational Mechanics and Analysis*, 73(1):31–51, 1980.

[19] D. Henry. Geometric theory of semilinear parabolic equations. *Lecture Notes in Mathematics*, 1981.

[20] T. W. Hiscock and S. G. Megason. Orientation of Turing-like patterns by morphogen gradients and tissue anisotropies. *Cell Systems*, 1(6):408–416, 2015.

[21] M. Holzer and A. Scheel. A slow pushed front in a Lotka–Volterra competition model. *Nonlinearity*, 25(7):2151–2179, jun 2012.

[22] R. E. Hunt and D. G. Crighton. Instability of flows in spatially developing media. *Proceedings: Mathematical and Physical Sciences*, 435(1893):109–128, 1991.

[23] C. K. R. T. Jones. *Geometric singular perturbation theory*, pages 44–118. Springer Berlin Heidelberg, Berlin, Heidelberg, 1995.

[24] T. Kapitula and K. Promislow. *Spectral and dynamical stability of nonlinear waves*, volume 457. Springer.

[25] T. W. Kibble. Topology of cosmic domains and strings. *Journal of Physics A: Mathematical and General*, 9(8):1387, 1976.

[26] E. Knobloch and R. Krechetnikov. Problems on time-varying domains: Formulation, dynamics, and challenges. *Acta Applicandae Mathematicae*, 137(1):123–157, 2015.

[27] L. Kramer, E. Ben-Jacob, H. Brand, and M. C. Cross. Wavelength selection in systems far from equilibrium. *Phys. Rev. Lett.*, 49:1891–1894, Dec 1982.

[28] M. Krupa and P. Szmolyan. Extending geometric singular perturbation theory to nonhyperbolic points—fold and canard points in two dimensions. *SIAM Journal on Mathematical Analysis*, 33(2):286–314, 2001.

[29] M. Krupa and P. Szmolyan. Extending slow manifolds near transcritical and pitchfork singularities. *Nonlinearity*, 14(6):1473–1491, sep 2001.

[30] R. Kuske and W. Eckhaus. Pattern formation in systems with slowly varying geometry. *SIAM Journal on Applied Mathematics*, 57(1):112–152, 1997.

[31] G. J. M. Marée. Slow passage through a pitchfork bifurcation. *SIAM Journal on Applied Mathematics*, 56(3):889–918, 1996.

[32] R. Monteiro. Horizontal patterns from finite speed directional quenching. *Discrete & Continuous Dynamical Systems-B*, 23(8):3503, 2018.

[33] R. Monteiro and A. Scheel. Phase separation patterns from directional quenching. *Journal of Nonlinear Science*, 27(5):1339–1378, 2017.

[34] M. Reed and B. Simon. *Methods of Modern Mathematical Physics. IV Analysis of Operators*. Academic Press, New York, 1978.

[35] I. Rehberg, E. Bodenschatz, B. Winkler, and F. H. Busse. Forced phase diffusion in a convection experiment. *Physical Review Letters*, 59(3):282, 1987.

[36] H. Riecke. Pattern selection by weakly pinning ramps. *EPL (Europhysics Letters)*, 2(1):1, 1986.

[37] H. Riecke and H.-G. Paap. Perfect wave-number selection and drifting patterns in ramped Taylor vortex flow. *Physical Review Letters*, 59(22):2570, 1987.

[38] M. Rietkerk, R. Bastiaansen, S. Banerjee, J. van de Koppel, M. Baudena, and A. Doelman. Evasion of tipping in complex systems through spatial pattern formation. *Science*, 374(6564):eabj0359, 2021.

[39] B. Sandstede and A. Scheel. Absolute and convective instabilities of waves on unbounded and large bounded domains. *Physica D: Nonlinear Phenomena*, 145(3-4):233–277, 2000.

[40] G. R. Sell and Y. You. *Dynamics of evolutionary equations*, volume 143. Springer, 2002.

[41] N. Stoop and J. Dunkel. Defect formation dynamics in curved elastic surface crystals. *Soft Matter*, 14(12):2329–2338, 2018.

[42] W. C. Troy. The role of Painlevé II in predicting new liquid crystal self-assembly mechanisms. *Arch. Ration. Mech. Anal.*, 227(1):367–385, 2018.

[43] W. H. Zurek. Cosmological experiments in superfluid helium? *Nature*, 317(6037):505–508, 1985.